



Chuanxiong Renshen Decoction Inhibits Alzheimer's Disease Neuroinflammation by Regulating PPAR γ /NF- κ B Pathway

Jinling Hou ^{1,*}, Xiaoyan Wang ^{1,*}, Jian Zhang¹, Zhuojun Shen¹, Xiang Li², Yuanxiao Yang²

¹School of Pharmacy, Hangzhou Medical College, Hangzhou, People's Republic of China; ²School of Basic Medical Sciences and Forensic Medicine, Hangzhou Medical College, Hangzhou, People's Republic of China

*These authors contributed equally to this work

Correspondence: Yuanxiao Yang; Xiang Li, Email yyx104475@163.com; leexiang2004@126.com

Background and Aim: Previous studies of our research group have shown that Chuanxiong Renshen Decoction (CRD) has the effect of treating AD, but the exact mechanism of its effect is still not clarified. The aim of this study was to investigate the effect and mechanism of CRD on AD neuroinflammation.

Materials and Methods: Morris Water Maze (MWM) tests were employed to assess the memory and learning capacity of AD mice. HE and Nissl staining were used to observe the neural cells of mice. The expression of Iba-1 and CD86 were detected by immunohistochemical staining. Utilize UHPLC-MS/MS metabolomics techniques and the KEGG to analyze the metabolic pathways of CRD against AD. Lipopolysaccharide (LPS) induced BV2 microglia cells to construct a neuroinflammatory model. The expression of Iba-1 and CD86 were detected by immunofluorescence and flow cytometry. The contents of TNF- α and IL-1 β were detected by ELISA. Western blot assay was used to detect the expression of PPAR γ , p-NF- κ B p65, NF- κ B p65 proteins and inflammatory cytokines iNOS and COX-2 in PPAR γ /NF- κ B pathway with and without PPAR γ inhibitor GW9662.

Results: CRD ameliorated the learning and memory ability of 3 \times Tg-AD mice, repaired the damaged nerve cells in the hippocampus, reduced the area of Iba-1 and CD86 positive areas in both the hippocampus and cortex regions, as well as attenuated serum levels of IL-1 β and TNF- α in mice. CRD-containing serum significantly decreased the expression level of Iba-1, significantly reduced the levels of TNF- α and IL-1 β , significantly increased the protein expression of PPAR γ , and significantly decreased the proteins expression of iNOS, COX-2 and p-NF- κ B p65 in BV2 microglia cells. After addition of PPAR γ inhibitor GW9662, the inhibitory effect of CRD-containing serum on NF- κ B activation was significantly weakened.

Conclusion: CRD can activate PPAR γ , regulating PPAR γ /NF- κ B signaling pathway, inhibiting microglia over-activation and reducing AD neuroinflammation.

Keywords: Alzheimer's disease, Chuanxiong Renshen Decoction, UHPLC-MS/MS, neuroinflammation, PPAR γ

Introduction

A progressive cognitive dysfunction and mental disorders characterize AD, a widespread central neurodegenerative disorder.¹ Age spots, with extracellular β -amyloid protein (A β) deposition as the nucleus, neurofibrillary tangles caused by hyperphosphorylation of intracellular tau protein, and neuron loss are the primary pathological alterations in the brain of AD patients.² Currently, there is a dearth of satisfactory therapeutic drugs for AD, and it is still necessary to find new therapeutic drugs for complex diseases with unclear etiology and multi-factor correlation.

More and more studies have confirmed that neuroinflammation is an indispensable key link in the upstream of AD pathogenesis³ and may be the deeper root cause of neurodegenerative diseases.⁴ The inflammatory response has now been extensively demonstrated in multiple studies of postmortem tissue samples from Alzheimer's disease.^{5–8} Many studies have highlighted that persistent inflammation in the brain can accelerate the progression of cognitive impairment,

triggering AD.^{9,10} Microglia are the main immune regulatory cells in the brain, and microglia and neuroinflammation play an important role in the occurrence and development of Alzheimer's disease.¹¹

CRD is a traditional Chinese medicine compound that has been clinically proven to have therapeutic effects on AD. We previously predicted through network pharmacology that CRD might regulate the MAPK pathway by intervening in the inflammatory response and other processes, possibly by down-regulating the CASP3 and EGFR targets to reduce the level of inflammation, so as to have therapeutic effects on Alzheimer's disease.¹²

Quantitative analysis of all metabolites in organisms, known as metabolomics, is a component of systems biology,¹³ which seeks to uncover the correlation between metabolites and pathological changes. In recent years, metabolomics techniques have been widely used for early screening of neurodegenerative diseases, such as AD, and to identify metabolic changes associated with disease progression.¹⁴ At present, metabolomics technology has detected a variety of biological metabolic markers related to AD, and has been widely used to explore the regulatory effects of Chinese medicines and compound formulas on related metabolic markers.^{15,16} UHPLC-MS/MS is one of the most widely used metabolomics techniques that can detect a large number of metabolic signatures from biological samples with high throughput and sensitivity.¹⁷

In this study, 3×Tg-AD mice were used as AD model mice and given CRD for three months. We used UHPLC-MS/MS to detect serum metabolites, and analyzed the potential serum biomarkers of CRD and the changes of related metabolic pathways. Then, the neuroinflammation model of BV2 microglia cells were established to verify the anti-inflammatory effect and mechanism of CRD *in vitro*.

Materials and Methods

Materials

Panax ginseng C. A. Meyer, Ligusticum chuanxiong hort, Pueraria lobata, Polygonum multiflorum Thunb. and Ginkgo biloba L. were all purchased from East China Medicine Co., LTD., lot No. 20210208. The samples were thoroughly verified by Associate Professor Yao Ying from the School of Pharmacy at Hangzhou Medical College, in accordance with the Chinese Pharmacopoeia 2020. The five herbs were crushed with a grinder and mixed according to the ratio of 1:2:2:2. The mixed herbs were heated with 8 volumes of (W/V) 60% ethanol for reflux 2 times for 2 hours each time.¹² Use a rotary evaporator to concentrate to the final concentration of 1.44 g/mL.

Animals and Treatment

Shanghai Nanfang Model Biotechnology Co., LTD. provided 3×Tg-AD mice and wild-type C57BL/6 mice, both weighing 25±5 g. From Hangzhou Medical College's Animal Experimental Center, 200±20 g male Sprague-Dawley rats were procured. Feeding conditions: constant temperature, temperature 22±1°C, light alternates every 12 hours, humidity 50%-60%, wind changes frequency 15–20 times/hour. Zhejiang Experimental Animal Center Experimental Animal Welfare Ethics Committee gave their approval for all the animal experiments conducted. C57BL/6 mice and SD rats both have the ethical approval number ZJCLA-IACUC-20020056 and ZJCLA-IACUC-20010190, respectively. All the animal procedures were performed in accordance with the Guidelines for Care and Use of Laboratory Animals of the National Institutes of Health.

Divided into two groups, the 6-month-old 3×Tg AD mice were allocated to Model and CRD, each containing 8 mice. The WT group was chosen from eight C57BL/6 mice aged 6 months. The CRD group mice were orally given CRD (14.4 g/kg/d), while the WT and Model groups of mice were administered an equivalent volume of physiological saline once daily for a duration of 3 months.¹⁸

After a 5-day period of adaptive feeding, 30 SD rats were randomly assigned into three groups (n=10 each): Normal rat serum group, CRD serum group, and Donepezil (DNPQ) serum group. The CRD serum group was given a dose of 10 g/kg/d, the DNPQ serum group was given a dose of 1.76 mg/kg/d, and the Normal rat serum group received administration of an equivalent volume of normal saline for a duration of 7 consecutive days.

Cell Culture and Treatment

Mouse BV2 microglial cells, purchased from iCell Bioscience Inc (Shanghai, China), were cultured in DMEM medium with 10% fetal bovine serum (Gibco) and 1% penicillin-streptomycin (Gibco) at 37°C with 5% CO₂. In the PPAR γ inhibition experiment, BV2 microglia cells were pretreated with CRD-containing serum (10%) and 10 μ M GW9662 (Sigma, USA) for 2 hours and then stimulated with LPS (100 μ g/mL) (Sigma, USA) for 22 hours.

Morris Water Maze (MWM) Test

Before administration, 1, 2, and 3 months after administration, the MWM test was employed to assess the learning and memory abilities of each group of mice. During the experiment, the water temperature was kept at (22 \pm 2)°C.

Brain Tissue Staining

Hippocampus tissue was taken from mice and fixed using a 4% paraformaldehyde solution. Paraffin wax was used to embed the tissues, then they were divided into sections. Xylene was used to dewax sections, then distilled water was used to wash them and hematoxylin and eosin were used to stain them. Finally, under an optical microscope (Eclipse E100, Nikon, Japan), histopathological alterations of the hippocampus were witnessed.

The brain sections were dewaxed with xylene, washed with distilled water, and soaked in 1% toluidine blue solution in an incubator at 50–60°C for 30 minutes. After dyeing, it was quickly differentiated with 95% ethanol, dehydrated with anhydrous ethanol, transparent with xylene and sealed with neutral glue.¹⁹ Finally, the optical microscope revealed the histopathological alterations of the hippocampus at last.

ELISA Analysis

The ELISA kit (ThermoFisher, USA) was employed to detect the IL-1 β and TNF- α contents of the serum of mice in each group, as per the manufacturer's instructions. The absorbance at 450 nm was detected by the cell imaging multifunctional detection system (CYTATION, BioTek, USA).

Immunohistochemical Assay

Paraffin sections of mouse brain tissue were roasted at 60°C for 20 minutes, then dewaxed and hydrated, and repaired with sodium citrate buffer (pH6.0) at high temperature and pressure.²⁰ Incubating the slices in a 3% H₂O₂ solution at room temperature for 25 minutes away from light, endogenous peroxidase was eliminated. After 3 washings with PBS (pH7.4), the sections were sealed with 3% BSA and incubated with specific primary antibody Iba-1 (1:200, Abcam, USA) and CD86 (1:200, bioss, Beijing) at 4°C overnight. The primary antibody was recovered, the slices were rinsed 3 times with PBS and then incubated at room temperature for half an hour with the secondary antibody (1:400, Abcam, USA). Wash the slices 3 times, shake dry and add freshly prepared DAB color developing solution to develop color, rinse with running water and wipe dry. Sections were re-dyed with hematoxylin for 3 minutes, rinsed with running water, dehydrated and sealed, and images were taken with an optical microscope.

UHPLC-MS/MS Detection

Sample Collection and Pretreatment

After the last administration, 24 mice (WT group, Model group, and CRD group) were collected for orbital venous blood. Centrifugation at 3000 r/min for 15 minutes at 4°C yielded serum.

The centrifuge tube was filled with 100 μ L of serum, followed by the addition of 400 μ L of an extraction solution (methanol: acetonitrile = 1:1, v/v) containing the isotope labeling standard.²¹ The mixture was then vortexed for a duration of 30 seconds. After the vortex, the samples were ultrasounded in an ice water bath for 10 minutes, and then stood at -40°C for 1 hour. Centrifugation at 4°C and 12000 rpm for 15 minutes was conducted on the sample, and then the supernatants were placed into the sample bottles for testing. In addition, an equal quantity of supernatant was drawn from all specimens and blended into a Quality Control (QC) sample for machine examination.

UHPLC-MS/MS Conditions

Vanquish ultra-high performance liquid chromatograph (UHPLC) (Thermo Fisher Scientific, USA) was used in this study.²² Using Waters ACQUITY UPLC BEH Amide liquid chromatography column (2.1 mm × 50 mm, 1.7 μm; Milford, MA, USA), the target compounds were divided. In liquid chromatography, the aqueous phase (Phase A) consists of 25 mmol/L ammonium acetate and 25 mmol/L ammonia water, while the organic phase (Phase B) is composed of acetonitrile.²³ The temperature of the sample tray was set to 4°C, while maintaining an injection volume of 2 μL.

The Orbitrap Exploris 120 mass spectrometer was equipped with electrospray ion sources (ESI). ESI parameter setting: the flow rate of the sheath gas was 50 Arb, while the auxiliary gas was 15 Arb; the spray voltage in the positive ion mode was 3800 V, while the negative ion mode was -3400 V. The capillary temperature was 320°C.

Data Processing

ProteoWizard software transforms the raw data into mzXML format, then R program package (with XCMS kernel) is employed for peak recognition, extraction, alignment, and integration processing.²⁴ Subsequently, it undergoes matching against the BiotreeDB (V2.1) self-constructed secondary mass spectrometry database for substance annotation, while setting the algorithm scoring cutoff value at 0.3.

The Effects of CRD-Containing Serum on BV2 Microglia Cells Were Detected

Preparation of the CRD-Containing Serum

After a 1-hour period of administering the last dose, the rats were subjected to anesthesia using pentobarbital sodium, and their abdominal aorta blood was then collected. Centrifugation of the blood at 3000 rpm for 15 minutes yielded serum after it had been left at room temperature for three hours. The serum was inactivated in a water bath at 56°C for 30 minutes, then sterilized by a 0.22 μm microporous filter and stored at -80°C for later use.

Cell Culture and Treatment

From iCell Bioscience Inc. in Shanghai, BV2 microglia cells were procured. Culturing of BV2 microglia cells with DMEM medium, supplemented with 1% penicillin/streptomycin and 10% fetal bovine serum, was conducted in an incubator with 5% CO₂ at 37°C. In the PPAR γ inhibition experiment, BV2 microglia cells were pretreated with CRD-containing serum (10%) and 10 μM GW9662 (Sigma, USA) for 2 hours and then stimulated with LPS (100 μg/mL) (Sigma, USA) for 22 hours.

Cell Viability Assay

The impact of CRD-containing serum on the viability of BV2 microglia cells was assessed using the MTT assay. The cells were inoculated at a concentration of 5000 cells per well into a 96 well plate, and set up a Normal rat serum group, a CRD serum group, and a Donepezil serum group. Each group cultured cells with 5 concentrations of serum (0%, 5%, 10%, 15%, 20%). After 24 hours of cell culture, in accordance with the manufacturer's directions, the MTT reagent (Beyotime, Shanghai, China) was employed to detect cell activity. The cell imaging multifunctional detection system was employed to gauge the absorbance at 490 nm.

Flow Cytometry

The expression of CD86 in BV2 microglia cells was detected by flow cytometry. BV2 microglia cells were inoculated into a six well plate, and set a control group (0 μg/mL), a LPS group (100 μg/mL), and a LPS group (200 μg/mL). After 24 hours of LPS stimulation, BV2 microglia cells were collected in a centrifuge tube. The cells were incubated with APC-conjugated monoclonal mouse CD86 antibody (MultiSciences, Hangzhou, China) at 4°C for 30 minutes away from light. PBS was used to clean the cells, then 500 μL PBS was added to re-suspend them. Cell suspensions were detected using a FACscan flow cytometer (BD FACS Celesta, USA). We used the Flowjo V10 software to analyze the data.

Immunofluorescence Staining

BV2 microglia cells were inoculated onto a glass slide in a six well plate (5×10^5 cells/well), and set up a control group, a LPS group, a CRD group, and a Donepezil group. The cells of the control group and the LPS group were cultured with

Normal rat serum (10%) for 2 hours, and the cells of the CRD group and the Donepezil group were cultured with CRD-containing (10%) serum and DNPQ-containing serum (10%) for 2 hours, respectively. Then, except the control group, cells in other groups were stimulated with LPS (100 µg/mL) for 22 hours. After 30 minutes of pre-cooling with 4% paraformaldehyde, the treated cells were permeated with 0.5% Triton-X for 2 minutes, then closed with goat serum for a further 30 minutes. Incubating the cells overnight with either Iba-1 (1:400, Abcam, USA) or NF-κB p65 (1:400, CST, USA) at 4°C was done. Incubating the cells at room temperature for an hour with an anti-rabbit secondary antibody (1:800, Abcam, USA) on the second day was done. The cells were stained with DAPI (Sigma, USA) for 2 minutes. Fluorescence quencher was added, and the fluorescence intensity of Iba-1 and NF-κB p65 was observed by the cell imaging multifunctional detection system.

Western Blot Analysis

The BCA protein assay was employed to ascertain the protein concentration from the cell lysates collected. The sodium dodecyl sulfate polyacrylamide gel electrophoresis (SDS-PAGE) was employed to separate the protein, which was then moved to polyvinylidene fluoride (PVDF) membranes. After a blocking solution had been incubated, PVDF membranes were left to be incubated overnight with specific primary antibodies. The next day, the membranes were incubated with anti-mouse or anti-rabbit secondary antibody (1:5000, proteintech, USA) at room temperature for 2 hours. The antibodies used were anti-COX-2 (proteintech, USA), anti-iNOS (proteintech, USA), anti-PPARγ (Cell Signaling Technology, USA), anti-phospho-NF-κB p65 (Cell Signaling Technology, USA), anti-NF-κB p65 (Cell Signaling Technology, USA), and anti-GAPDH (proteintech, USA). The images were captured and recorded by the high sensitivity chemiluminescence imaging system (Amersham ImageQuant 800, cytiva, USA). Analysis software of high sensitivity chemiluminescence imaging system was utilized for the purpose.

Statistical Analysis

The images and experimental data were processed using SPSS 24.0 software (IBM Corp., Armonk, NY, USA) and GraphPad Prism 10. The inter-group mean and statistical results were compared using one-way analysis of variance (ANOVA). The experimental data were expressed as mean ± SD. $P < 0.05$ was considered statistically significant.

Results

CRD Ameliorated the Learning and Memory Ability of 3×Tg-AD Mice

The Model group's escape latency was significantly greater than the WT group's before administration ($p < 0.01$), and their number of platform crossings was significantly less than that of the WT group ($p < 0.05$) (Figure 1A). The CRD group's escape latency was significantly decreased ($p < 0.01$, $p < 0.01$, $p < 0.05$) (Figure 1B–D) after 1, 2 and 3 months of administration, compared to the Model group, while the number of platform crossings was significantly augmented ($p < 0.05$, $p < 0.05$, $p < 0.01$). Results showed that 3×Tg AD mice had significantly ameliorated their learning and memory abilities due to CRD.

CRD Repaired Hippocampal Neuronal Damage in 3×Tg AD Mice

The results of HE staining (Figure 2A) showed that hippocampal nerve cells in WT group had abundant cytoplasm, clear nuclear structure, and light staining. The Model group mice, aged nine months, exhibited a decrease in nerve cells, staining intensified, and the nuclear structure was indistinct. The CRD group's cytoplasm of nerve cells was much more abundant, with a greater number and a clearer nuclear structure than the Model group, following a 3-month period of continuous administration.

Results from the Nissl staining of the mice hippocampus (Figure 2B) indicated a great abundance of neurons in the CA1 region of the WT group's hippocampus. Compared with the WT group, the number of neurons in the hippocampus of the Model group was significantly reduced, the arrangement was loose, and the staining was deepened. After 3 months of constant administration, the CRD group's hippocampal neuron count rose in comparison to the model group, and their nuclear structure was discernible.

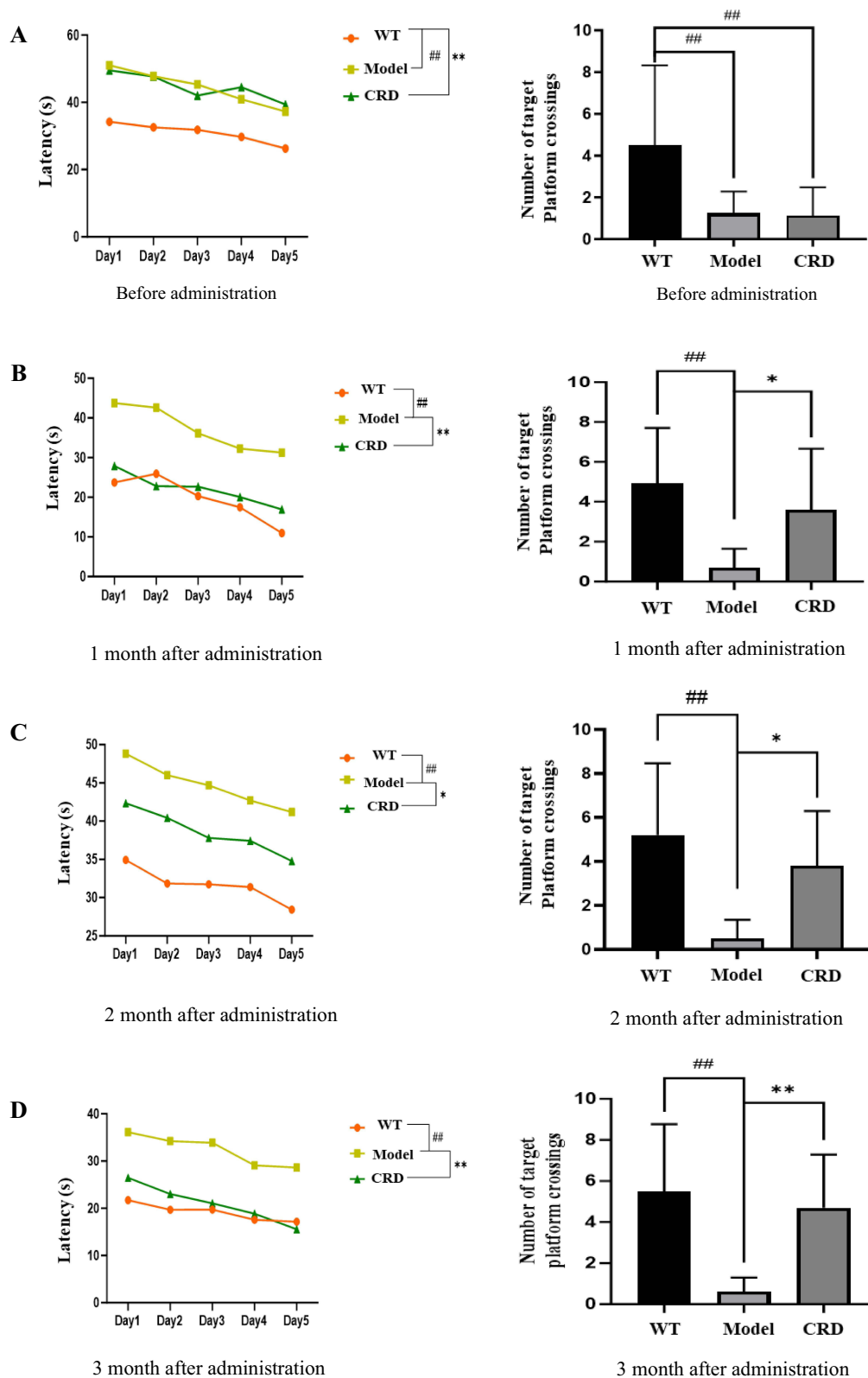


Figure 1 Effects of CRD on escape latency and number of times crossing platforms in 3xTg-AD mice. (A) Before administration, (B) 1 month after administration, (C) 2 month after administration, (D) 3 month after administration. Data are expressed as the mean from 8 mice per group, ###*p*<0.01 versus the WT group; **p*<0.05, ***p*<0.01 versus the Model group.

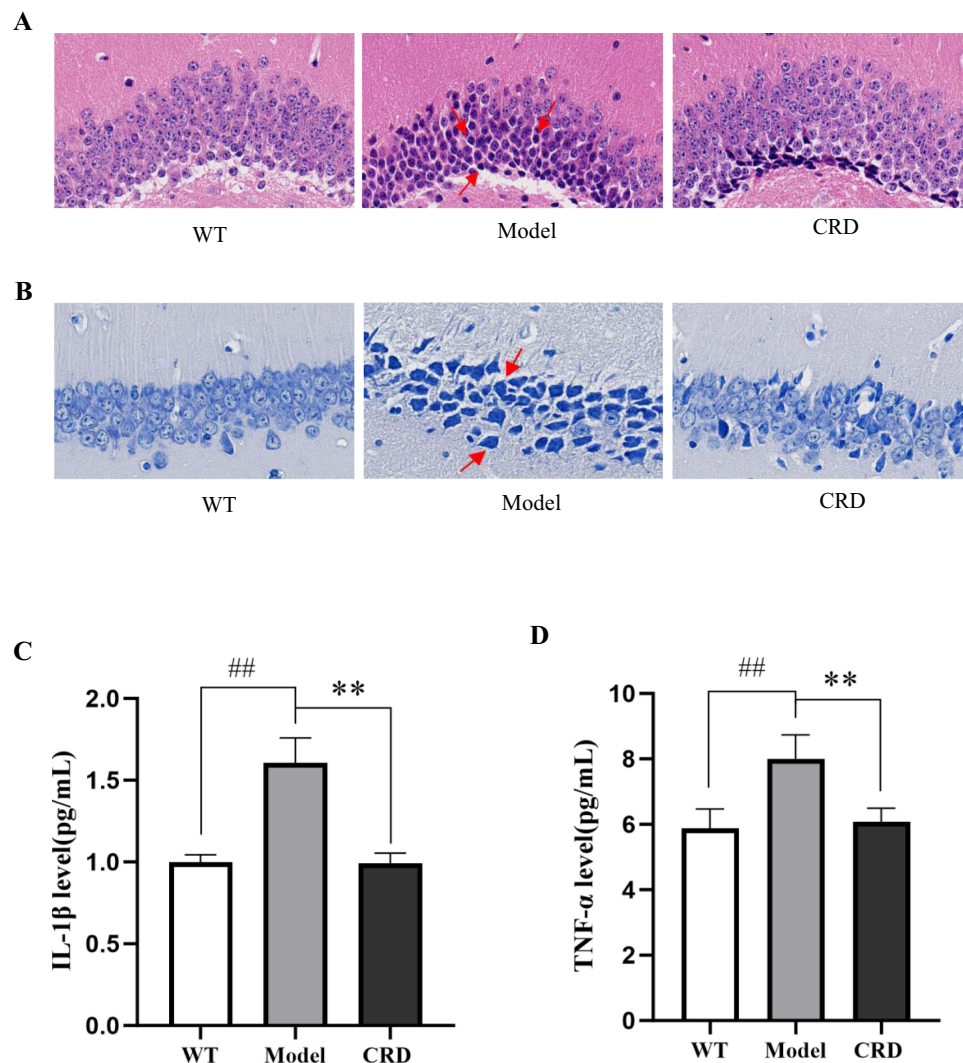


Figure 2 CRD repaired hippocampal neuronal damage in 3 \times Tg-AD mice. **(A)** HE staining showed the pathological changes of DG region in hippocampal tissue of mice in each group (n=6, Scale bar=50 μ m). **(B)** Nissl staining showed the pathological changes of CA1 region in hippocampal tissue of mice in each group (n=6, Scale bar=50 μ m). **(C)** Effect of CRD on levels of IL-1 β in 3 \times Tg-AD mice serum. **(D)** Effect of CRD on levels of TNF- α in 3 \times Tg-AD mice serum. Data are presented as the mean \pm SD (n=6), ### p <0.01 versus the WT group; ** p <0.01 versus the Model group.

CRD Decreased the Levels of Inflammatory Cytokines in Serum of 3 \times Tg-AD Mice

Investigation of the expression of inflammatory cytokines (IL-1 β , TNF- α) was conducted through ELISA. The Model group's levels of inflammatory cytokines were significantly higher than the WT group, as demonstrated by Figure 2C and D (p <0.01, p <0.01). After 3 months of administration, the levels of inflammatory cytokines were significantly decreased in the CRD group compared with the Model group (p <0.01, p <0.01).

CRD Inhibited the Activation of Microglia Cells in Cortex and Hippocampus in 3 \times Tg AD Mice

Immunohistochemical staining of Iba-1 (Figure 3A) showed that compared with WT group, the percentage of Iba-1 positive area in cortex and hippocampus of mice in Model group significantly increased (p <0.01), cell body enlarged, staining deepened and synapses thickened. After CRD administration, the percentage of Iba-1 positive area in cortex and hippocampus of mice significantly decreased (p <0.01), the cell body became smaller, and the synapses became thinner.

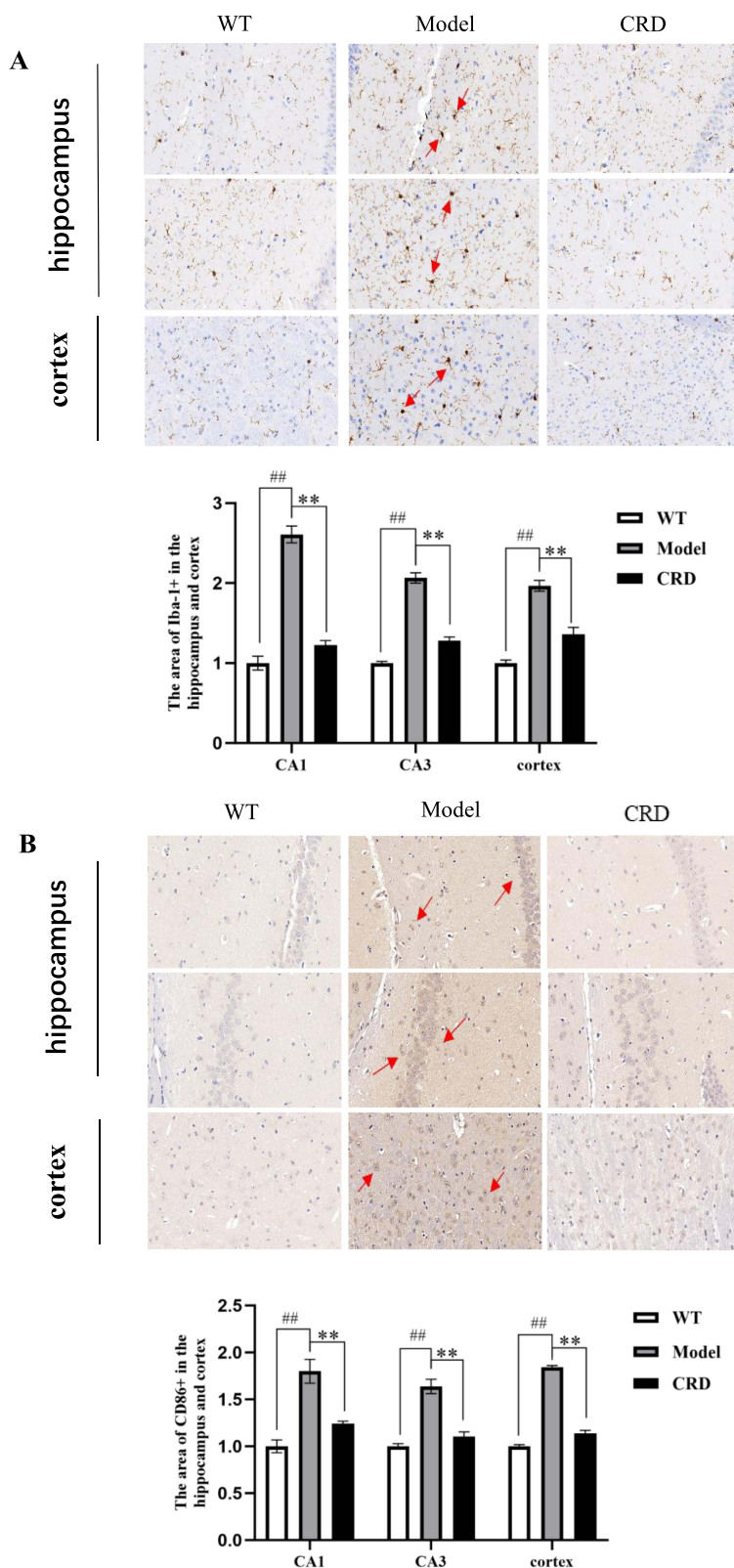


Figure 3 Effect of CRD on activation of microglia in hippocampus and cortex of mice. **(A)** The expression of Iba-1 in the hippocampus and cortex of mice (Scale bar=20µm). **(B)** The expression of CD86 in the hippocampus and cortex of mice (Scale bar=20µm). Data are presented as the mean ± SD (n=5), ^{##}p<0.01 versus the WT group; ^{**}p<0.01 versus the Model group.

The percentage of CD86 positive area in Model group significantly increased ($p < 0.01$) in comparison to WT group, as demonstrated by the results of CD86 immunohistochemical staining (Figure 3B). The cortex and hippocampus of mice experienced a marked decrease ($p < 0.01$) in the percentage of CD86 positive area following CRD administration.

Effect of CRD on Metabolic Profile of 3×Tg AD Mice

QC for UHPLC-MS/MS Analysis

The total ion spectrum showed that both in POS (Figure 4A) and NEG (Figure 4B) modes, the peak RT and peak area of QC samples exhibit good overlap, indicating that the analysis system has good stability. The QC samples exhibited significant aggregation in the PCA score chart (Figure 4C and D), indicating good repeatability of the analysis system.

Multivariate Statistical Analysis of Serum Metabolomics

To identify the intrinsic differences between the WT, Model, and CRD groups, we performed a multivariate analysis using SIMCA software (V16.0.2, Sartorius Stedim Data Analytics AB, Umea, Sweden). The PCA score chart showed that the samples in the WT and Model groups was clearly separated, and the clustering effect was relatively obvious, and the measurements of all samples fell within the 95% confidence interval (Figure 5A). The samples in the Model group and CRD group also showed equally significant clustering effects (Figure 5B). In order to better discover true differences between groups and screen for efficacious differences metabolites, we constructed an OPLS-DA model for analysis. The scatter plot of OPLS-DA model scores (Figure 5C and D) exhibited a pronounced segregation between the WT group and Model group, as well as between the Model group and CRD group. In order to avoid overfitting of the OPLS-DA test model, a replacement test was carried out. The replacement test results showed that the intercepts of R2Y and Q2 were 0.91 and -0.77, respectively, in the WT vs Model group (Figure 5E), and 0.93 and -0.63, respectively, in the Model vs CRD group (Figure 5F), indicating that the OPLS-DA model was not overfitting. The high quality and reliability of the OPLS-DA Model were validated, indicating that it was appropriate for this study to investigate the disparities between the WT and Model groups, as well as between the Model and CRD groups.

Identification of Differential Metabolites

An online database was used to screen metabolites with statistical differences. According to the conditions of $p < 0.05$ and $VIP > 1$, 3421 differential metabolites were screened in the WT vs Model group, of which 2693 showing up-regulated and 728 displaying down-regulated. In the Model vs CRD group, 2936 differential metabolites were screened, of which 945 showing up-regulated and 1991 displaying down-regulated. The screened differential metabolites were visualized by the volcano map (Figure 6A and B). We calculated the Euclidean distance matrix for the quantitative values of the differential metabolites, clustering the differential metabolites using the complete linkage method, and displaying them with thermal maps (Figures S1 and S2). The WT vs Model group clustered 161 differential metabolites, and the Model vs CRD group clustered 183 differential metabolites. Their intersection included 88 differential metabolites, which were shown using the Venn diagram (Figure 6C). Among them, 84 different metabolites were consistent with the change trend. Specific differential metabolite information is shown in Table 1. In addition L-phenylalanine,^{25,26} LysoPC(22:0), LysoPC(22:1(13Z)), LysoPC(14:0/0:0), LysoPC(24:1(15Z))²⁷ may be related to the anti-AD neuroinflammatory effect of CRD.

Metabolic Pathway Analysis

The metabolic pathways of 84 potential biomarkers were analyzed using the Kyoto Encyclopedia of Genes and Genomes (KEGG) and MetaboAnalyst 5.0. As shown in Figure 6D, 15 metabolic pathways were collectively enriched by differential metabolites. Studies have found that metabolic pathways related to AD include Arginine biosynthesis,²⁸ Taurine and hypotaurine metabolism,²⁹ PPAR signaling pathway,³⁰ Glycerophospholipid metabolism,³¹ and Linoleic acid metabolism. Among them, the PPAR signaling pathway is closely related to neuroinflammation.^{32,33}

Effect of CRD-Containing Serum on BV2 Microglia Cells

Effects of CRD-Containing Serum on the Viability of BV2 Microglia Cells

MTT assay revealed the viability of BV2 microglia cells. In the Normal rat serum group, the cell viability in the 20% Normal rat serum group was significantly higher than that in the 10% fetal bovine serum group ($p < 0.05$), but no

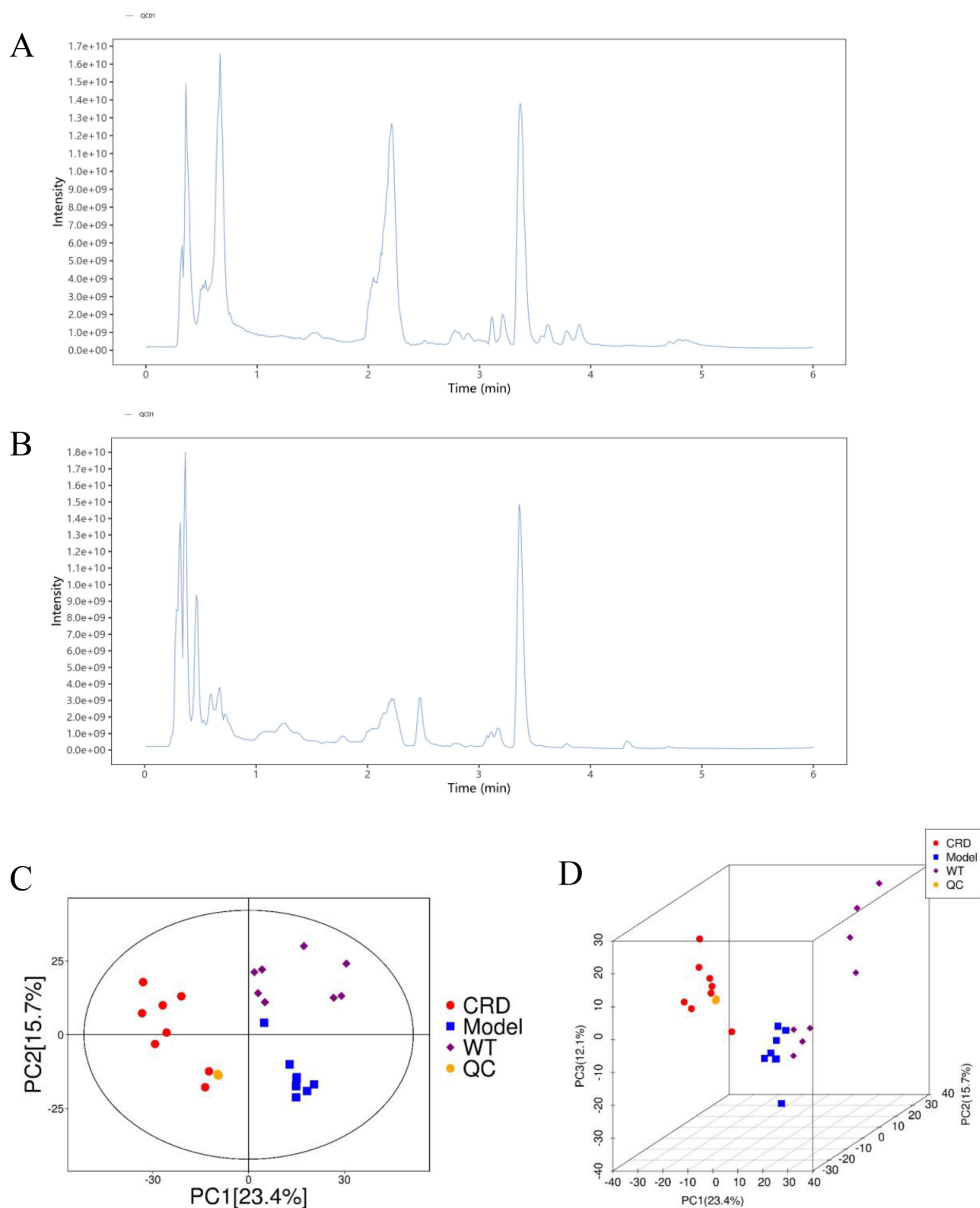


Figure 4 QC of UHPLC-MS/MS analysis. (A) TIC (POS), (B) TIC (NEG); (C) Two-dimensional PCA for QC, (D) Three-dimensional PCA for QC.

noteworthy distinction was observed between the other groups and the 10% fetal bovine serum group (Figure 7A). In the CRD serum group and the Donepezil serum group, the cell viability of the 20% CRD serum group and the 20% Donepezil serum group was significantly higher than that of the 10% Normal rat serum group ($p < 0.01$, $p < 0.01$), while no

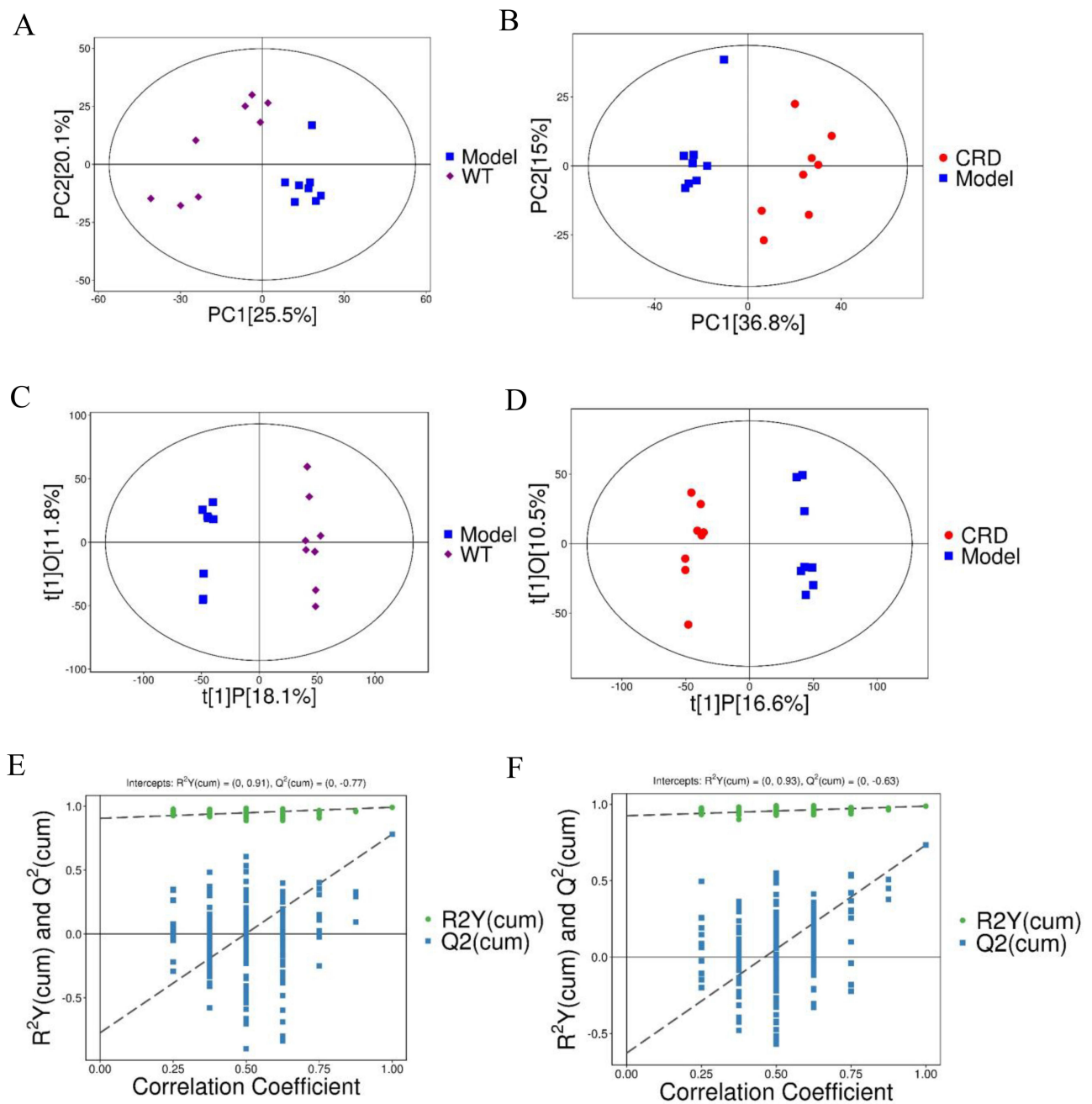


Figure 5 Multivariate analysis of serum metabolomics. (A) PCA (WT vs Model), (B) PCA (Model vs CRD); (C) OPLS-DA (WT vs Model), (D) OPLS-DA (Model vs CRD); (E) statistical validation of OPLS-DA (WT vs Model), (F) statistical validation of OPLS-DA (Model vs CRD).

noteworthy divergence was observed between the other groups and the 10% Normal rat serum group (Figure 7B). Therefore, 10% CRD-containing serum and 10% Donepezil-containing serum were selected for subsequent experiments.

Construction of Neuroinflammatory Model of BV2 Microglia Cells

The Iba-1 protein is specifically expressed in microglia cells of the central nervous system and serves as a marker for BV2 microglia cell activation.^{34,35} The results of immunofluorescence staining (Figure 8A) showed that compared with the 0 $\mu\text{g}/\text{mL}$ LPS group, the fluorescence intensity of Iba-1 in BV2 microglia cells stimulated by 100 $\mu\text{g}/\text{mL}$ or 200 $\mu\text{g}/\text{mL}$ LPS for 24 h was significantly enhanced ($p < 0.01$, $p < 0.01$).

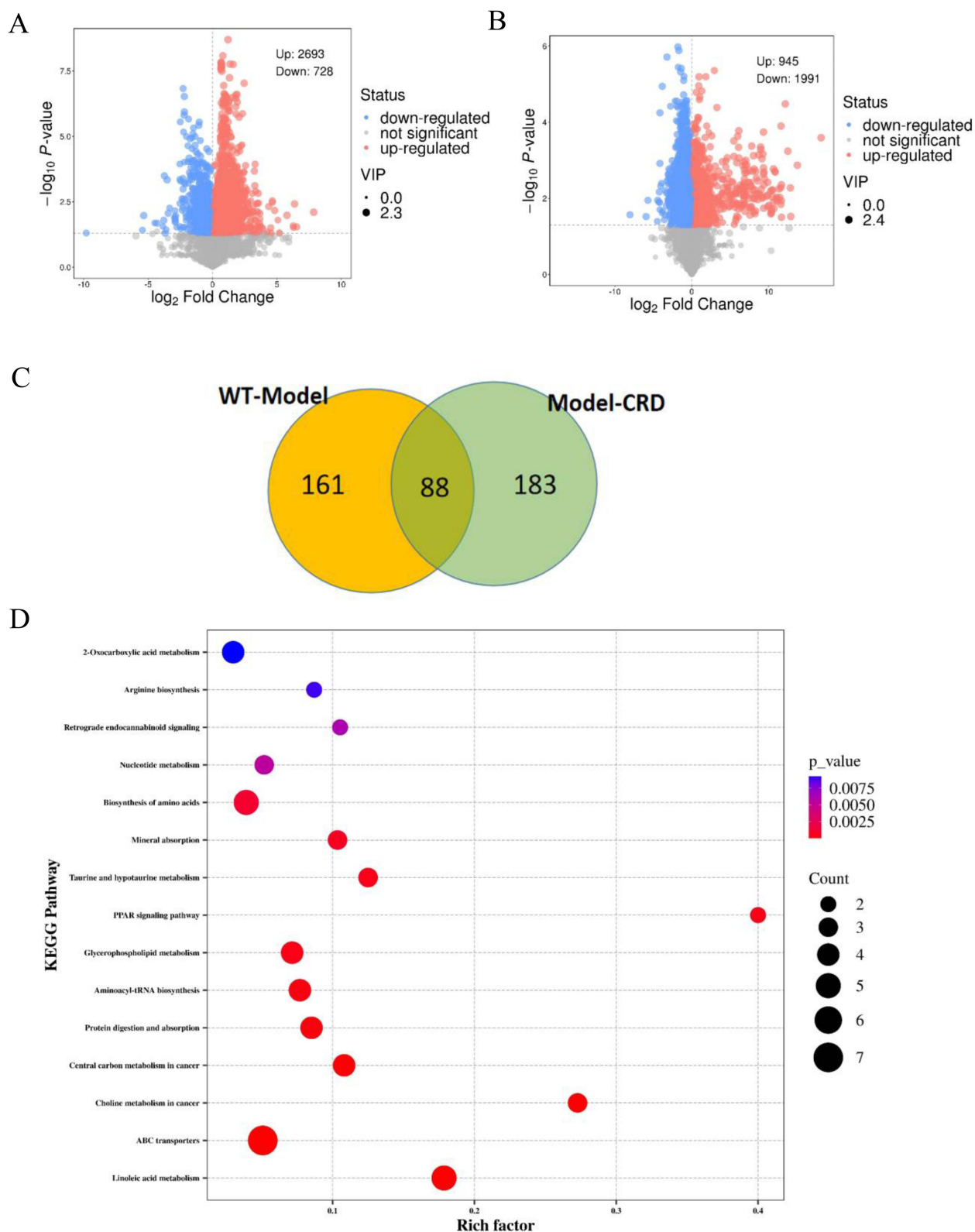


Figure 6 Volcano plot for the differentially expressed metabolites. **(A)** WT vs Model, **(B)** Model vs CRD. **(C)** Venn diagram of metabolites in different comparison groups. **(D)** KEGG pathway enrichment map of differential metabolites.

Table I Identification of Potential Biomarkers in Serum of Mice in WT Group, Model Group and CRD Group

NO.	Metabolites	RT	m/z	p value		Trend	
				WT-Model	Model-CRD	WT-Model	Model-CRD
1	L-Allothreonine	217.5385	118.0511	0.002444	0.03029319	↑	↓
2	Norvaline	190.0535	118.0862	0.026058	0.03931801	↑	↓
3	Allopurinol-1-ribonucleoside	137.02	269.0883	0.006935	0.003897122	↑	↓
4	DL-Phenylalanine	166.136	166.0861	0.019032	0.015682795	↑	↓
5	2-Hydroxy-3-methylbutyric acid	81.4176	117.056	0.028631	7.04E-05	↑	↓
6	2-Hydroxybutyric acid	122.425	103.0354	4.89E-05	0.000518341	↑	↓
7	L-Phenylalanine	166.982	164.0718	0.009389	0.008621751	↑	↓
8	L-Tyrosine	190.095	182.0812	0.00817	0.007704546	↑	↓
9	PC(22:5(7Z,10Z,13Z,16Z,19Z)/20:1(11Z))	37.0286	862.629	0.001451	0.003469802	↑	↓
10	8-Hydroxy-2'-deoxyguanosine	168.239	282.085	0.007765	0.003518609	↑	↓
11	Pyrrolidine	190.044	72.08092	0.006199	0.028059356	↑	↓
12	1,3-Dihydro-(2H)-indol-2-one	19.04835	134.0599	0.002314	0.006063825	↑	↓
13	Guanosine	167.098	284.0987	0.007134	0.004426019	↑	↓
14	PC(22:6(4Z,7Z,10Z,13Z,16Z,19Z)/16:0)	39.54345	806.5712	0.021347	0.007364973	↑	↓
15	PE(16:0/18:2(9Z,12Z))	44.67615	714.5098	0.019223	0.0275545	↑	↓
16	PC(16:0/14:0)	43.5875	706.5377	0.020289	0.048199391	↑	↓
17	PC(18:1(11Z)/14:0)	22.5024	732.5532	0.004938	0.006098751	↑	↓
18	PC(22:2(13Z,16Z)/14:1(9Z))	22.36515	784.5823	0.006014	0.010709675	↑	↓
19	PC(20:2(11Z,14Z)/14:0)	136.3825	758.5704	0.003069	0.047220458	↑	↓
20	Taurine	223.7695	126.0221	0.000335	0.000250706	↑	↓
21	PC(P-18:1(9Z)/16:1(9Z))	22.3569	742.5729	0.002467	0.013602206	↑	↓
22	Isobutyryl-L-carnitine	166.809	232.1545	0.040607	0.001399422	↑	↓
23	PC(20:3(8Z,11Z,14Z)/15:0)	42.269	770.569	0.026027	0.000854495	↑	↓
24	Perillic acid	33.2295	165.0925	0.00098	0.001005851	↓	↑
25	PC(18:2(9Z,12Z)/14:0)	42.9578	730.5375	0.025204	0.001032323	↑	↓
26	Propionylcarnitine	178.5075	218.139	0.03008	0.000852913	↑	↓
27	Phthalic acid	247.152	165.0198	7.03E-07	0.000472719	↑	↓
28	2-(Ethylamino)-4,5-dihydroxybenzamide	220.175	197.0894	0.002414	0.002566963	↑	↓
29	Alpha-dimorphelic acid	29.4681	279.232	0.014275	0.036833374	↑	↓
30	2-Hydroxyethanesulfonate	110.626	124.9916	0.009527	0.01443377	↓	↑
31	9,10-DHOME	33.9849	313.2386	0.005067	0.006778288	↑	↓
32	Choline	165.049	104.1068	0.003772	0.002570521	↑	↓
33	PC(22:6(4Z,7Z,10Z,13Z,16Z,19Z)/20:5(5Z,8Z,11Z,14Z,17Z))	144.0385	852.5667	0.001678	0.007281265	↑	↓
34	L-Glutamine	284.1265	147.0765	0.037817	0.003068495	↓	↑
35	13S-hydroxyoctadecadienoic acid	29.307	295.2281	0.030043	0.033862345	↑	↓
36	Maleic acid	233.681	115.004	0.001497	0.035246959	↑	↓
37	PC(20:1(11Z)/15:0)	41.1138	774.5986	0.00131	0.009092302	↑	↓
38	PC(24:1(15Z)/14:0)	42.1516	816.6426	0.01061	0.011522467	↑	↓
39	Nicotinamide N-oxide	75.36175	139.0503	0.002251	0.024271413	↓	↑
40	2-O-(4,7,10,13,16,19-Docosahexaenoyl)-1-O-hexadecylglycero-3-phosphocholine	38.046	792.5919	0.01516	0.02686344	↑	↓
41	N-Acetylserine	243.04	148.0606	0.013064	0.001413866	↑	↓

(Continued)

Table I (Continued).

NO.	Metabolites	RT	m/z	p value		Trend	
				WT-Model	Model-CRD	WT-Model	Model-CRD
42	16-Hydroxy hexadecanoic acid	30.00365	271.2284	0.030896	0.002849996	↑	↓
43	2,4-Dihydroxybenzoic acid	17.35725	153.0197	0.001247	0.005731883	↑	↓
44	L-Valine	208.442	116.072	0.00289	0.005169754	↑	↓
45	N-Acetylmethionine	219.97	173.0935	0.002359	0.000232934	↑	↓
46	(alpha-D-mannosyl)7-beta-D-mannosyl-diacetylchitobiosyl-L-asparagine, isoform A (protein)	223.074	90.0551	0.025809	0.000414337	↑	↓
47	Eicosapentaenoic acid	24.3443	301.2173	0.000241	0.017730465	↑	↓
48	O-Acetyl-L-serine	243.1945	146.0461	0.043964	0.002218371	↑	↓
49	PC(20:4(5Z,8Z,11Z,14Z)/16:0)	345.5675	782.5676	0.043964	0.002218371	↑	↓
50	Hypotaurine	211.1025	110.0271	0.021223	0.00422521	↑	↓
51	1,2-Dihydroxy-3-keto-5-methylthiopentene	49.9043	163.0423	0.006833	0.00923327	↑	↓
52	2-Piperidone	30.85775	100.0758	0.004664	8.75E-05	↑	↓
53	2-Methoxy-4-vinylphenol	43.9167	149.0609	0.034126	0.047809685	↑	↓
54	Thymidine	41.1207	241.0833	0.009442	0.035061145	↓	↑
55	Stearidonic acid	22.0381	275.2022	2.65E-05	0.000342812	↑	↓
56	PC(22:5(4Z,7Z,10Z,13Z,16Z)/14:0)	22.2613	780.5538	6.29E-05	0.000347102	↑	↓
57	PC(14:0/20:1(11Z))	260.645	760.5823	0.003042	0.039950931	↑	↓
58	N-a-Acetyl-L-arginine	224.507	217.1298	0.014987	0.002293792	↑	↓
59	LysoPE(18:1(9Z)/0:0)	135.204	478.294	0.000525	0.003125952	↑	↓
60	PC(18:0/14:1(9Z))	42.1081	732.5539	0.004597	0.003424753	↑	↓
61	6-Hydroxy-1H-indole-3-acetamide	27.8273	191.0812	0.007355	0.043400792	↓	↑
62	Alanyl-Isoleucine	237.932	203.1393	0.000385	0.004485892	↑	↓
63	2-Acetylthiazole	186.6985	128.0177	0.031904	0.025061242	↑	↓
64	3-Methylglutaryl-L-carnitine	242.212	290.1604	0.005477	0.037998048	↓	↑
65	PC(18:2(9Z,12Z)/16:0)	22.37705	758.5706	0.00329	0.02841967	↑	↓
66	Histidinal	52.5304	140.0817	0.007975	0.011018442	↑	↓
67	PC(14:1(9Z)/20:0)	23.05805	760.5815	0.000634	0.017865813	↑	↓
68	Proline betaine	173.0915	144.1021	0.009001	0.000368687	↑	↓
69	13-L-Hydroperoxylinoleic acid	118.284	311.2231	0.000985	0.031363989	↑	↓
70	L-Fucose	80.04135	163.0613	0.000149	0.003855631	↑	↓
71	Gallic acid	85.7831	169.0121	0.002258	0.015796487	↓	↑
72	N-gamma-Glutamyl-S-allylcysteine	220.883	291.1049	0.04429	0.040314785	↑	↓
73	8-isoprostaglandin E2	43.7292	351.2182	0.006177	0.002986768	↑	↓
74	L-Erythrulose	148.8405	119.0352	0.033307	0.020704188	↑	↓
75	Aspartame	211.049	295.1265	0.002292	0.012222709	↑	↓
76	Acetone cyanohydrin	47.912	86.06019	0.002292	0.012222709	↑	↓
77	PC(18:3(6Z,9Z,12Z)/15:0)	44.42255	742.5371	0.047825	0.042115246	↑	↓
78	LysoPC(22:0)	124.4945	580.4322	0.002754	0.012459694	↑	↓
79	Hypogeic acid	24.66475	253.2172	0.001009	0.034010889	↑	↓
80	LysoPC(24:0)	123.097	608.4655	0.001944	0.043663802	↑	↓
81	Inositol 1,3,4-trisphosphate	179.096	420.9712	0.022608	0.041980695	↓	↑
82	LysoPC(22:1(13Z))	125.149	578.4185	0.003974	0.000258684	↑	↓
83	LysoPC(24:1(15Z))	123.794	606.4475	0.000514	0.002538298	↑	↓
84	LysoPC(14:0/0:0)	135.053	468.3083	0.001328	0.001653896	↑	↓

Note: ↑: Differential metabolite up-regulation; ↓: Differential metabolite down-regulation.

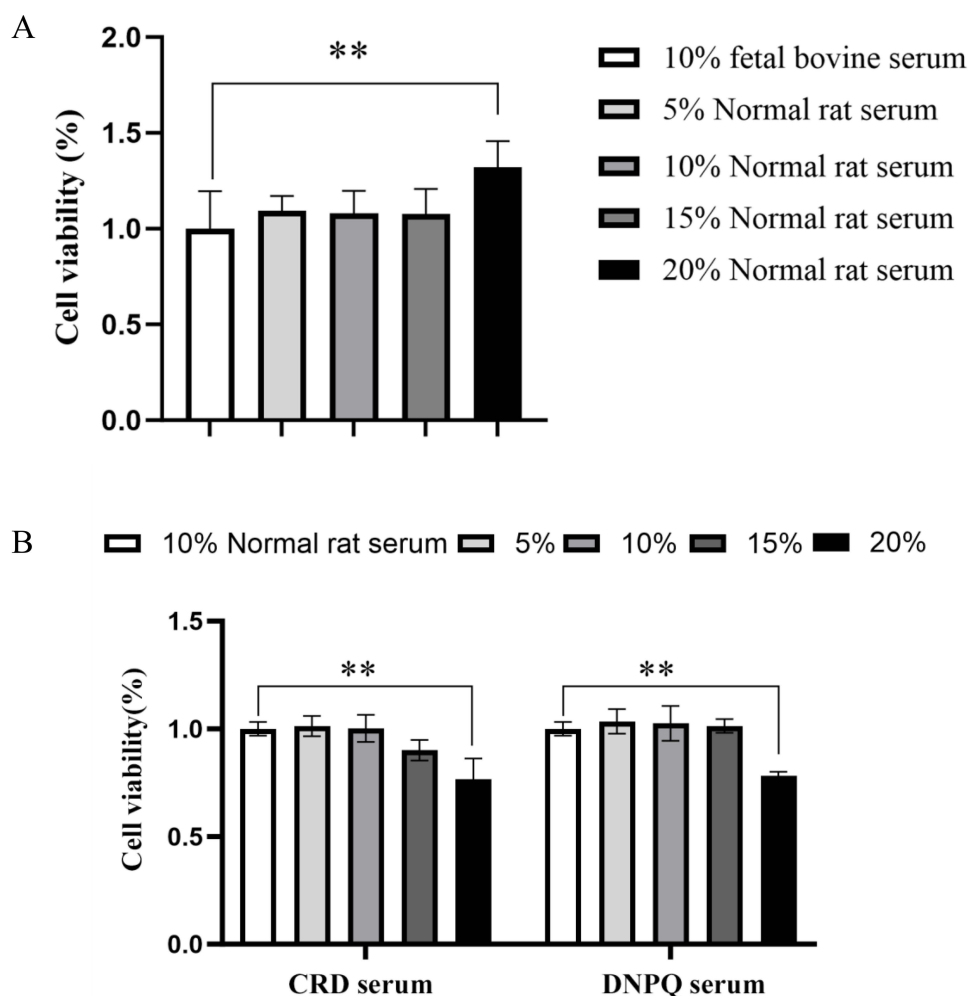


Figure 7 Effect of CRD-containing serum on BV2 microglia cells viability. **(A)** Effects of the Normal rat serum on BV2 microglia cells viability. Data are presented as the means \pm SD (n=6). **(B)** Effects of the CRD-containing and the Donepezil-containing serum on BV2 microglia cells viability. Data are presented as the mean \pm SD (n=6). ** p <0.01 versus the 10% Normal serum.

CD86 is a marker for proinflammatory microglia cells.^{36,37} The expression of CD86 was assessed using flow cytometry. The results demonstrated a significant upregulation of CD86 expression in BV2 microglia cells following 24 hours stimulation with LPS at concentrations of 100 μ g/mL and 200 μ g/mL compared to unstimulated BV2 microglia cells (p <0.01, p <0.01) (Figure 8B).

The stimulation of LPS can lead to the translocation of NF- κ B p65 into the nucleus. The expression of NF- κ B p65 was assessed via Western blot analysis. The results showed that compared with BV2 microglia cells without LPS stimulation, the expression of NF- κ B p65 in the nucleus of BV2 microglia cells after 24 hours stimulation with 100 μ g/mL LPS was significantly increased (p <0.01) (Figure 8C). Therefore, LPS with a concentration of 100 μ g/mL was selected to stimulate BV2 microglia cells for 24 hours as a neuroinflammatory cell model.

CRD-Containing Serum Inhibited the Activation of BV2 Microglia Cells

The expression of Iba-1 protein in BV2 microglia cells was detected by immunofluorescence assay. A comparison of the LPS group to the control group revealed a significant rise in Iba-1 protein expression (p <0.01) (Figure 9A and B). The CRD group's expression of Iba-1 protein was significantly diminished in comparison to the LPS group (p <0.01). The results demonstrated that the activation of BV2 microglia cells was effectively inhibited by CRD.

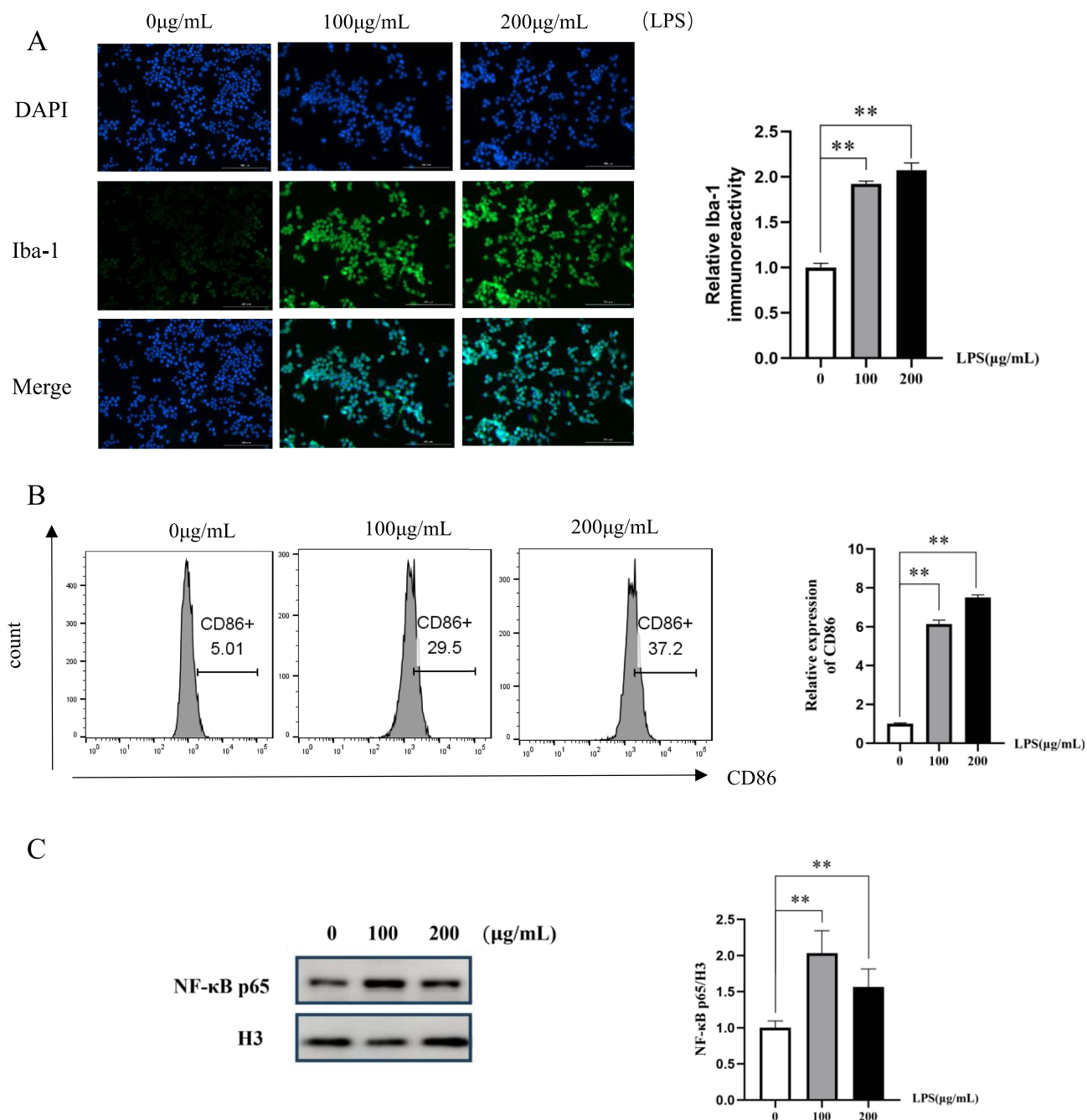


Figure 8 Effects of LPS on expression of Iba-1, CD86 and NF-κB p65 in BV2 microglia cells. **(A)** The expression of Iba-1 in LPS-induced BV2 microglia was detected by immunofluorescence assay (Scale bar=200μm). **(B)** The expression of CD86 in BV2 microglia cells induced by LPS was measured via flow cytometry. **(C)** The protein expression of NF-κB p65 in BV2 microglia cell nucleus induced by LPS were detected via Western blot analysis. Data are presented as the mean ± SD (n=5), **p<0.01 versus the 0 μg/mL LPS group.

CRD-Containing Serum Reduced the Expression of COX-2 and iNOS in LPS-Stimulating BV2 Microglia Cells
 Regulatory factors iNOS and COX-2, of great significance in inflammatory response, foster the production of inflammatory mediators. Western blot results showed a marked up-regulation in the expression of COX-2 and iNOS in the LPS group compared to the control group ($p<0.01$, $p<0.01$) (Figure 10A–C). A significant down-regulation in COX-2 and iNOS expression was observed in the CRD group in comparison to the LPS group ($p<0.01$, $p<0.01$).

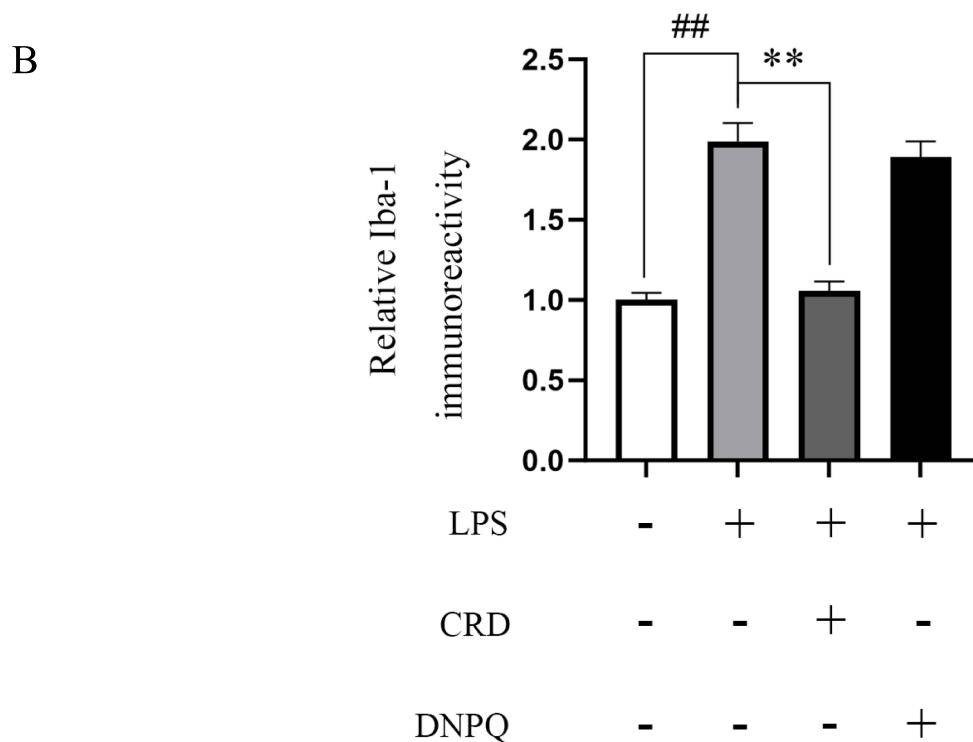
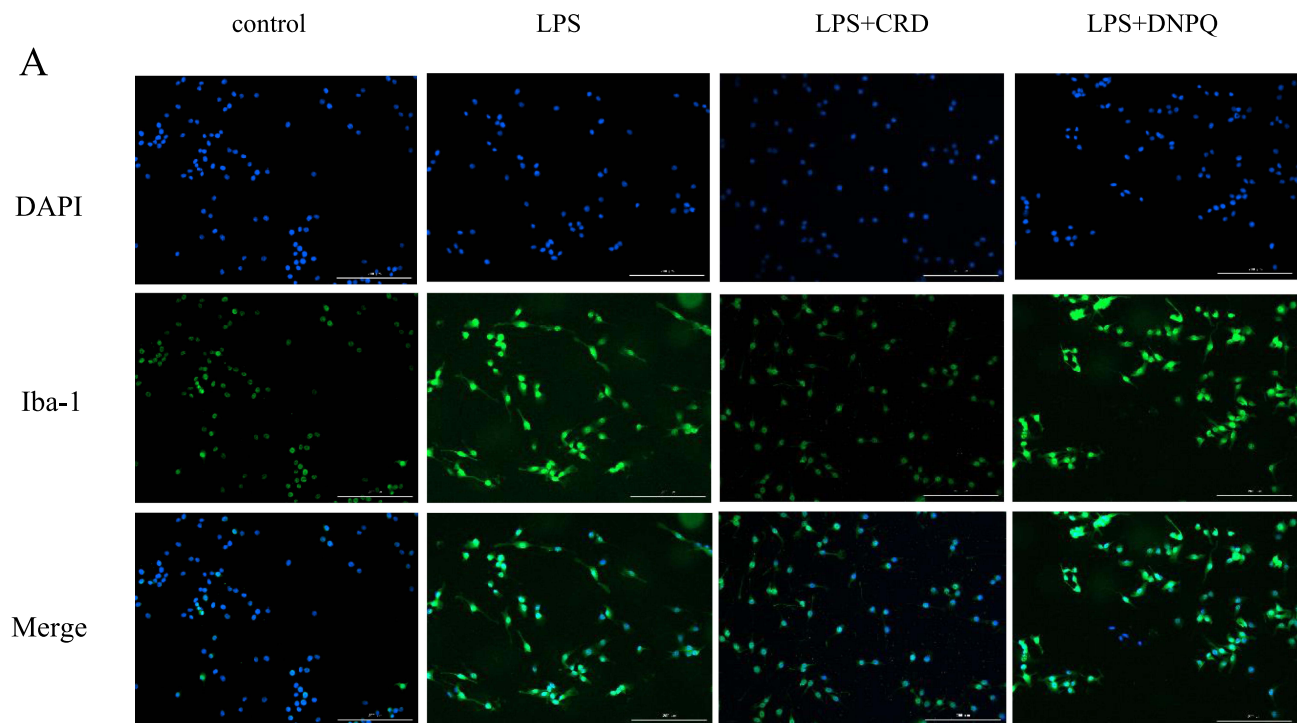


Figure 9 Effect of CRD-containing serum on the expression of Iba-1 in BV2 microglia cells. (**A** and **B**) Immunofluorescence analysis of Iba-1 proteins in BV2 microglia cells (Scale bar=200 μ m). Data are presented as the mean \pm SD (n=6), $^{###}p<0.01$ versus the control group; $^{**}p<0.01$ versus the LPS group.

CRD-Containing Serum Reduced Neuroinflammation by Regulating the PPAR γ /NF- κ B Pathway

PPAR γ plays a significant role in reducing neuroinflammation, and its agonists reduce the production of inflammatory cytokines.³⁸ PPAR γ significant decreased in protein expression in LPS stimulated BV2 microglia cells ($p<0.01$)

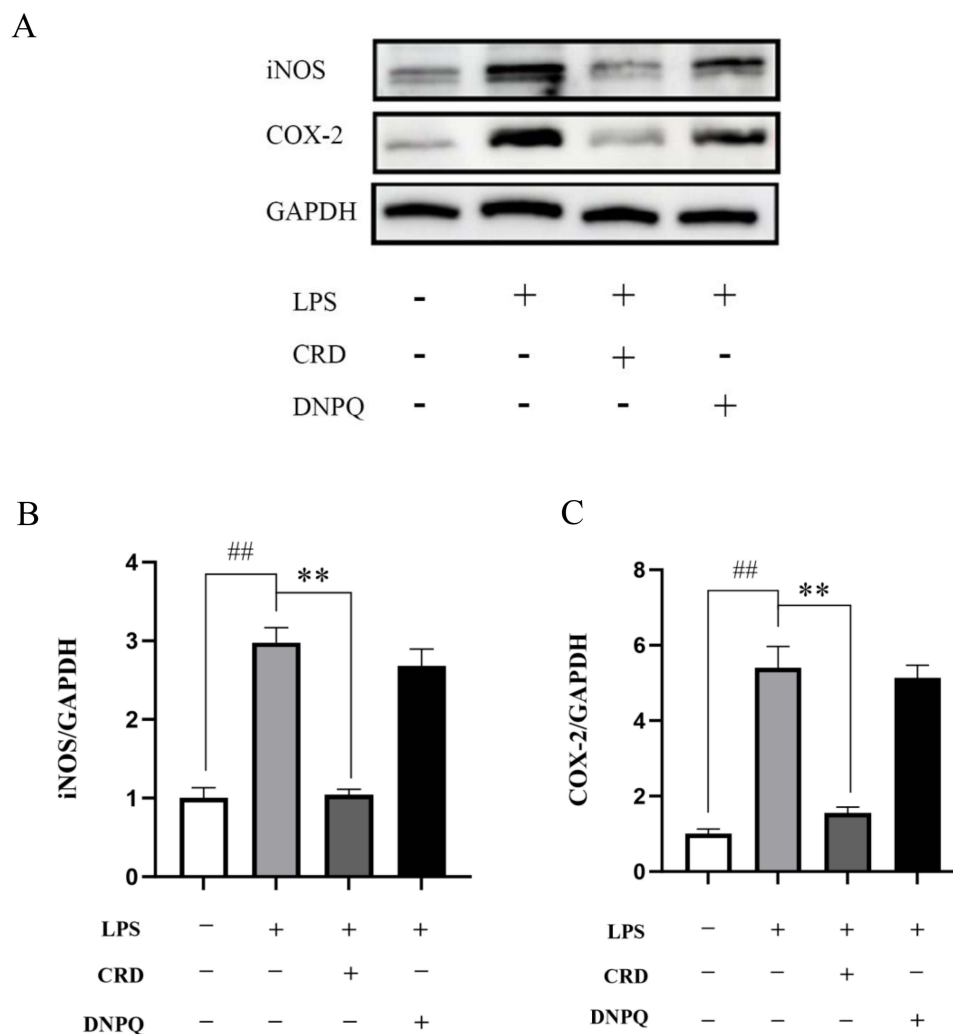


Figure 10 Effect of CRD-containing serum on the expression levels of iNOS and COX-2 protein in BV2 microglia cells. **(A)** Western blot analysis of protein expression in BV2 microglia cells, the expression levels of **(B)** iNOS and **(C)** COX-2. Data are presented as the mean \pm SD (n=5), ### p <0.01 versus the control group; ** p <0.01 versus the LPS group.

(Figure 11A), while its expression was enhanced by CRD-containing serum (p <0.01). After inhibition of PPAR γ with GW9662, the expression of PPAR γ protein decreased significantly (p <0.01).

Research has revealed that LPS combines with Toll-like receptor 4 (TLR4) on microglia cells, thereby activating the NF- κ B signaling pathway.³⁹ As a major transcriptional regulator, NF- κ B can induce the transcription of proinflammatory cytokines.⁴⁰ A significant increase in NF- κ B p65 phosphorylation was observed in the LPS group when compared to the control group (p <0.01), as demonstrated by Figure 11B. The CRD group showed a marked decrease in NF- κ B p65 phosphorylation when compared to the LPS group (p <0.01). However, after addition of PPAR γ inhibitor GW9662, CRD-containing serum lost its regulatory effect on LPS-induced NF- κ B pathway in BV2 microglia cells, showing that the level of NF- κ B p65 phosphorylation was significantly increased (p <0.01).

Immunofluorescence was utilized to observe the relocation of NF- κ B p65 from the cytoplasm to the nucleus. The red fluorescence in the nucleus of the LPS group was observed to be enhanced compared to the control group, as depicted in Figure 11C indicating translocation of NF- κ B p65 from the cytoplasm to the nucleus. Compared with the LPS group, the red fluorescence in the nucleus of CRD group was weakened, indicating that CRD exhibits inhibitory effects on the translocation of NF- κ B p65 into the nucleus. However, after addition of GW9662, CRD drug-containing serum lost its regulatory effect on LPS-induced NF- κ B pathway in BV2 microglia cells, showing enhanced NF- κ B p65 nuclear translocation.

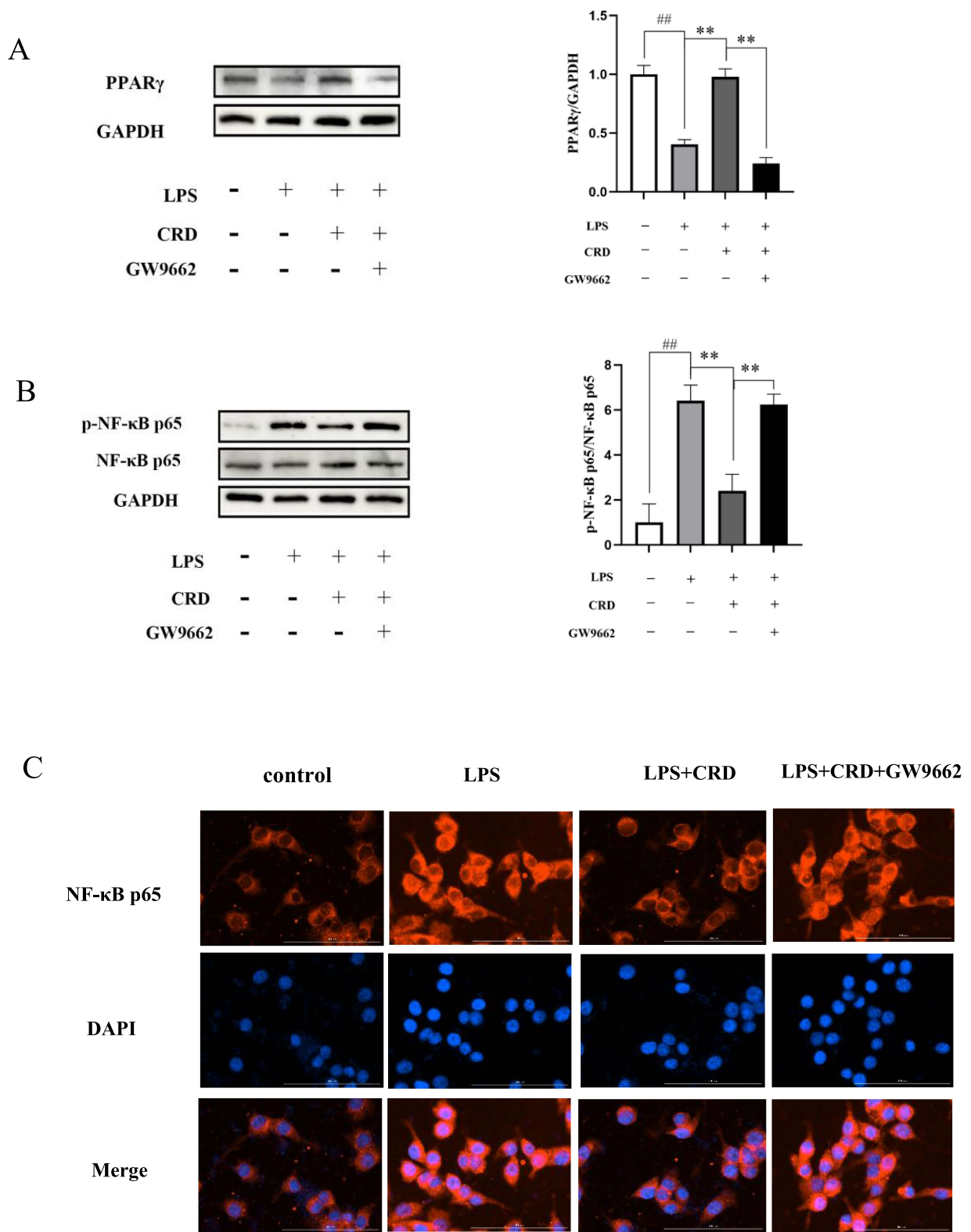


Figure 11 Effect of CRD-containing serum on PPAR γ /NF- κ B pathway. **(A)** The protein expression level of PPAR γ in BV2 microglia cells was determined by Western blotting. **(B)** The protein expression level of NF- κ B p65 and p-NF- κ B p65 in BV2 microglia cells was determined by Western blotting. Data are presented as the mean \pm SD (n=5), ^{###}p<0.01 versus the control group; ^{**}p<0.01 versus the CRD group. **(C)** Immunofluorescence analysis of p65 proteins in BV2 microglia cells (Scale bar=100 μ m).

Discussion

3×Tg-AD mice, widely utilized in AD research, serve as a fundamental tool. The 6-month-old 3×Tg-AD mice exhibited cognitive decline, and A β plaques and neuroinflammation were detected in their hippocampus.⁴¹ Hence, *in vitro* investigations were conducted using 3×Tg-AD mice as AD animal models to elucidate the mechanistic for the anti-AD effects of CRD. MWM test, pathological section staining, inflammation detection and immunohistochemistry are all important methods to study anti-AD drugs.

In this study, the anti-AD effects of CRD on AD model mice were investigated. The results suggest that CRD can enhance memory and learning in mice, repair damaged hippocampal neurons, suppress microglial activation in the hippocampus and cortex, and reduce IL-1 β and TNF- α levels in mouse serum. These findings imply that the anti-AD effect of CRD may be attributed to its anti-inflammatory properties. The anti-AD mechanism of CRD was further studied based on UHPLC-MS/MS metabolomics. The results showed that the differential metabolites screened were involved in the different mechanisms of action of CRD against AD. L-glutamine is involved in the glutamate-glutamine cycle, whose homeostasis is critical for synaptic function.^{42,43} The most relevant pathological factor of cognitive decline in AD patients is synaptic dysfunction that occurs at an early stage.⁴⁴ We observed that the level of L-glutamine was significantly decreased in the Model group, and significantly increased after CRD treatment. This suggests that the anti-AD effect of CRD may be achieved by maintaining homeostasis of the glutamate-glutamine cycle.

The central cholinergic system is closely related to AD and is involved in learning and memory activities.^{45,46} AD related cholinergic dysfunction is characterized by decreased acetylcholine (Ach) content and choline acetylase (ChAT) activity and increased acetylcholinesterase (AChE) activity.^{47,48} This feature leads to elevated levels of choline in the blood circulation and synaptic gap. In this study, we found that the choline level of mice in the Model group was significantly increased, which is consistent with the above views. After treatment with CRD, choline levels decreased significantly, which predicted that CRD might enhance ChAT activity and weaken AChE activity, thus promoting the synthesis of Ach and inhibiting the decomposition of Ach.

Numerous studies have unequivocally substantiated the key role of A β theory in the nosogenesis of AD, and the accumulation of A β outside nerve cells to form age plaques, also known as amyloid plaques, is one of the main pathological characteristics of AD.^{49,50} Under normal circumstances, a homeostatic equilibrium is maintained between the production and degradation of A β . However, in AD symptoms, too much A β is produced, and when it is not cleaned up in time, amyloid plaques form in brain tissue.⁵¹ Gallic acid (GA), a phenolic molecule, mitigated cognitive decline in APP/PS1 transgenic mice by reducing A β ₁₋₄₂ aggregation and neurotoxicity.⁵²⁻⁵⁴ In this study, gallic acid levels were significantly reduced in the Model group, while significantly enhanced in the CRD group.

Numerous recent studies have elucidated the key role of neuroinflammation in the onset and progression of AD, and chronic inflammation in the brain is one of the pathological characteristics of AD.^{55,56} In the state of inflammation, microglia cells are activated and discharge pro-inflammatory factors, such as IL-1 β and TNF- α , which damage peripheral neurons and ultimately lead to impaired learning and memory ability.

Therefore, reducing inflammation is considered to be an important way to treat AD. Lysophosphatidylcholine (LPC) is a molecule related to neurodegeneration and demyelination generated by the hydrolysis of phosphatidylcholine (PC) through phospholipase A2 (PLA2),⁵⁷ which can cause activation of inflammasomes (NLRP3, NLRC4) in microglia cells and astrocytes.⁵⁸ Research has shown that PLA2 levels increase under pathological conditions in AD.^{59,60} As a product of PLA2 activity, the level of LPC increases under AD pathology,^{61,62} thus increasing the formation of A β oligomers,⁶³ which directly leads to neuroinflammation and neurodegeneration.⁶⁴ In this study, the levels of LysoPC (22:0), LysoPC (22:1 (13Z)), LysoPC (14:0/0:0) and LysoPC (24:1 (15Z)) in the Model group were significantly increased, consistent with previous studies. After treatment with CRD, the levels of these metabolites significantly decreased, suggesting that the anti-AD neuroinflammation effect of CRD is related to lipid and amino acid metabolism. We found that CRD could reduce the levels of IL-1 β and TNF- α in serum of 3×Tg-AD mice, which predicted the anti-AD neuroinflammation effect of CRD.

In vitro, we prepared CRD-containing serum from rats and used LPS-induced BV2 microglia cells as neuroinflammatory model to explore the anti-inflammatory effects of CRD. Immunofluorescence analysis and Western blot analysis

showed that CRD-containing serum could inhibit the expression of Iba-1 and CD86, markers of BV2 microglia cells activation, and the expression of pro-inflammatory cytokine COX-2 and iNOS. Therefore, we conclude that CRD-containing serum alleviates neuroinflammation by inhibiting microglial activation and excessive release of pro-inflammatory mediators.

NF- κ B is a critical element in both *in vivo* and *in vitro* neuroinflammatory activity, and plays a pivotal role in the pathogenesis of neurodegenerative diseases through its regulation of microglia-mediated neuroinflammation.⁶⁵ Abnormal regulation of NF- κ B in BV2 microglia cells is associated with overproduction of pro-inflammatory mediators.⁶⁶ When BV2 microglia cells are stimulated by LPS, NF- κ B p65 transpositions into the nucleus and regulates gene transcription of the pro-inflammatory mediators COX-2 and iNOS.⁶⁷ Our results suggest that CRD-containing serum reduces the phosphorylation level and nuclear translocation of NF- κ B p65. Therefore, we conclude that CRD-containing serum improves neuroinflammation by inhibiting NF- κ B signaling.

The nuclear transcription factor PPAR γ , activated by a ligand, regulates the transcription of multiple genes and is implicated in anti-inflammatory processes.⁶⁸ PPAR γ can reduce the expression of COX-2 and iNOS, so as to reduce neuroinflammation.⁶⁹ In this study, we found that PPAR γ protein expression was down-regulated in LPS-induced BV2 microglia cells, while CRD-containing serum treatment significantly increased PPAR γ protein expression.

In Beas-2B cells and rat lung tissue, the inhibitory effect of curcumin on NF- κ B was dependent on up-regulation of PPAR γ activity.⁷⁰ Histone deacetylase 3 (HDAC3) inactivates NF- κ B by upregulating PPAR γ , thereby reducing inflammation and inhibiting atherosclerosis.⁷¹ By inhibiting the activation of NF- κ B, the PPAR γ activator (+) - (R, E)-6A1 exhibits anti-inflammatory effects.⁷² Strychnine significantly inactivates PPAR γ , and then NF- κ B is activated, reducing the release of pro-inflammatory factors.⁷³ It can also mediate NF- κ B degradation and promote NF- κ B export from the nucleus. In this study, we found that CRD-containing serum inhibited the activation of NF- κ B pathway in LPS-induced BV2 microglia cells. After treatment with PPAR γ inhibitors, CRD-containing serum did not inhibit the activation of NF- κ B pathway in LPS-induced BV2 microglia cells.

In summary, our study showed that after CRD treatment, the learning and memory ability of 3xTg-AD mice was significantly ameliorated, the number of positive cells of Iba-1 and CD86 in hippocampus and cortical regions was significantly reduced, and the levels of proinflammatory mediators COX-2 and iNOS in serum were significantly decreased. Serum metabolomics analysis by UHPLC-MS/MS suggested that the mechanism of CRD against AD neuroinflammation may be realized through PPAR signaling pathway. The results of cell experiments showed that CRD-containing serum significantly reduced the number of Iba-1 positive cells in BV2 microglia cells, decreased the expression levels of COX-2 and iNOS proteins, significantly increased the expression of PPAR γ protein, and inhibited the activation of NF- κ B pathway in BV2 microglia cells. To sum up, CRD has an anti-AD effect, and its mechanism of action is through the activation of PPAR γ , thereby inhibiting NF- κ B pathway.

There are still some limitations in our study. We only used one neuroinflammatory cell model to study. After that, we will construct AD cell models with A β 1-42 and Okadaic acid (OA) induced cells respectively to further verify the anti-AD effect of CRD and make the experimental results more convincing. In addition, we will also establish a co-culture system of microglia and neuronal cells to assess the effect of CRD on activating microglia-mediated neuronal apoptosis.

Conclusion

CRD can improve the learning and memory of 3xTg-AD mice and neuroinflammation in the brain. The mechanism may be through regulating the activation of PPAR γ , regulating the PPAR γ /NF- κ B signaling pathway, inhibiting the over-activation of microglia, and reducing the neuroinflammation of AD.

Acknowledgments

This work was supported by 2024 National Health Commission Scientific Research Fund- Zhejiang Province Health Key Science and Technology Plan Project (NO. WKJ-ZJ-2422) and Basic research business expenses of Hangzhou Medical College (NO. KYZD202006).

Author Contributions

All authors contributed to data analysis, drafting or revising the article, have agreed on the journal to which the article will be submitted, gave final approval of the version to be published, and agree to be accountable for all aspects of the work.

Disclosure

The authors report no conflicts of interest in this work.

References

1. Jack CR, Bennett DA, Blennow K, et al. NIA-AA research framework: toward a biological definition of alzheimer's disease. *Alzheimers Dement*. 2018;144(4):535–562. doi:10.1016/j.jalz.2018.02.018
2. Hosseinzadeh H, Sadeghnia HR, Ghaeni FA, et al. Effects of saffron (*Crocus sativus* L) and its active constituent, crocin, on recognition and spatial memory after chronic cerebral hypoperfusion in rats. *Phytother Res*. 2012;263(3):381–386. doi:10.1002/ptr.3566
3. Pascoal TA, Benedet AL, Ashton NJ, et al. Microglial activation and tau propagate jointly across Braak stages. *Nat Med*. 2021;279(9):1592–1599. doi:10.1038/s41591-021-01456-w
4. Gulen MF, Samson N, Keller A, et al. cGAS-STING drives ageing-related inflammation and neurodegeneration. *Nature*. 2023;6207973(7973):374–380. doi:10.1038/s41586-023-06373-1
5. Beardmore R, Hou R, Darekar A, et al. The locus coeruleus in aging and alzheimer's disease: a postmortem and brain imaging review. *J Alzheimers Dis*. 2021;831(1):5–22. doi:10.3233/JAD-210191
6. Rossano SM, Kreisler WC. Untangling the relationship between microglia and tau in Alzheimer's disease. *Trends Neurosci*. 2021;4412(12):927–929. doi:10.1016/j.tins.2021.10.002
7. Franco-Bocanegra DK, George B, Lau LC, et al. Microglial motility in Alzheimer's disease and after A β 42 immunotherapy: a human post-mortem study. *Acta Neuropathol Common*. 2019;71(1):174. doi:10.1186/s40478-019-0828-x
8. Chen C, Liao J, Xia Y, et al. Gut microbiota regulate Alzheimer's disease pathologies and cognitive disorders via PUFA-associated neuroinflammation. *Gut*. 2022;7111(11):2233–2252. doi:10.1136/gutjnl-2021-326269
9. Kou JJ, Shi JZ, He YY, et al. Luteolin alleviates cognitive impairment in Alzheimer's disease mouse model via inhibiting endoplasmic reticulum stress-dependent neuroinflammation. *Acta Pharmacol Sin*. 2022;434(4):840–849. doi:10.1038/s41401-021-00702-8
10. Bradburn S, Murgatroyd C, Ray N. Neuroinflammation in mild cognitive impairment and Alzheimer's disease: a meta-analysis. *Ageing Res Rev*. 2019;50:1–8. doi:10.1016/j.arr.2019.01.002
11. Singh D. Astrocytic and microglial cells as the modulators of neuroinflammation in Alzheimer's disease. *J Neuroinflammation*. 2022;191(1):206. doi:10.1186/s12974-022-02565-0
12. Shen ZJ, Fu YB, Hou JL, et al. Integrating network pharmacology, UPLC-Q-TOF-MS and molecular docking to investigate the effect and mechanism of Chuanxiong Renshen decoction against Alzheimer's disease. *Chin Med*. 2022;171(1):143. doi:10.1186/s13020-022-00698-1
13. Marchev AS, Vasileva LV, Amirova KM, et al. Metabolomics and health: from nutritional crops and plant-based pharmaceuticals to profiling of human biofluids. *Cell Mol Life Sci*. 2021;7819–7820(19–20):6487–6503. doi:10.1007/s00018-021-03918-3
14. Lista S, González-Domínguez R, López-Ortiz S, et al. Integrative metabolomics science in Alzheimer's disease: relevance and future perspectives. *Ageing Res Rev*. 2023;89:101987. doi:10.1016/j.arr.2023.101987
15. Wang A, Shi M, Xing J, et al. Treatment effects of Radix ginseng-Schisandra chinensis herb pair on Alzheimer's disease: an investigation of MS-based metabolomics investigation. *J Pharm Biomed Anal*. 2022;220:115007. doi:10.1016/j.jpba.2022.115007
16. Wei M, Liu Z, Liu Y, et al. Urinary and plasmatic metabolomics strategy to explore the holistic mechanism of lignans in *S. chinensis* in treating Alzheimer's disease using UPLC-Q-TOF-MS. *Food Funct*. 2019;109(9):5656–5668. doi:10.1039/C9FO00677J
17. Poorna Basuri P, Vijayakumar R, Nalini CN. Estimation of minoxidil in human plasma using UHPLC-MS/MS and its application in pharmacokinetic study. *J Chromatogr B Analyt Technol Biomed Life Sci*. 2022;1192:123104. doi:10.1016/j.jchromb.2022.123104
18. Wu Q, Miao X, Zhang J, et al. Astrocytic YAP protects the optic nerve and retina in an experimental autoimmune encephalomyelitis model through TGF- β signaling. *Theranostics*. 2021;1117(17):8480–8499. doi:10.7150/thno.60031
19. Dai S, Wei J, Zhang H, et al. Intermittent fasting reduces neuroinflammation in intracerebral hemorrhage through the Sirt3/Nrf2/HO-1 pathway. *J Neuroinflammation*. 2022;191(1):122. doi:10.1186/s12974-022-02474-2
20. Wang Y, Chen Y, Xin J, et al. Metabolomic profiles of the liquid state fermentation in co-culture of *Eurotium amstelodami* and *Bacillus licheniformis*. *Front Microbiol*. 2023;14:1080743. doi:10.3389/fmicb.2023.1080743
21. Dai J, Cai J, Zhang T, et al. Transcriptome and metabolome analyses reveal the mechanism of corpus luteum cyst formation in pigs. *Genes*. 2023;2:1410. doi:10.3390/genes14101848
22. Lv S, Dai W, Zheng Y, et al. Anxiolytic effect of YangshenDingzhi granules: integrated network pharmacology and hippocampal metabolomics. *Front Pharmacol*. 2022;13:966218. doi:10.3389/fphar.2022.966218
23. Yang F, Wu SC, Ling ZX, et al. Altered plasma metabolic profiles in Chinese patients with multiple sclerosis. *Front Immunol*. 2021;12:792711. doi:10.3389/fimmu.2021.792711
24. Liu P, Yang Q, Yu N, et al. Phenylalanine metabolism is dysregulated in human hippocampus with alzheimer's disease related pathological changes. *J Alzheimers Dis*. 2021;832:609–622. doi:10.3233/JAD-210461
25. Wang X, Sun G, Feng T, et al. Sodium oligomannate therapeutically remodels gut microbiota and suppresses gut bacterial amino acids-shaped neuroinflammation to inhibit Alzheimer's disease progression. *Cell Res*. 2019;2910(10):787–803. doi:10.1038/s41422-019-0216-x
26. Peña-Bautista C, Álvarez-sánchez L, Roca M, et al. Plasma lipidomics approach in early and specific alzheimer's disease diagnosis. *J Clin Med*. 2022;11(4):1117. doi:10.3390/jcm11041117

27. Zhu R, Lei Y, Shi F, et al. Arginine Reduces Glycation in $\gamma(2)$ Subunit of AMPK and pathologies in alzheimer's disease model mice. *Cells*. 2022;11(7):1121. doi:10.3390/cells11071121
28. He Y, Wang Y, Liu S, et al. A metabolomic study of the urine of rats with Alzheimer's disease and the efficacy of Ding-Zhi-Xiao-Wan on the afflicted rats. *J Sep Sci*. 2020;438(8):1458–1465. doi:10.1002/jssc.201900944
29. Qu X, Guan P, Han L, et al. Levistolidine A attenuates alzheimer's pathology through activation of the PPAR γ pathway. *Neurotherapeutics*. 2021;18(1):326–339. doi:10.1007/s13311-020-00943-1
30. Meng S, Li S, Chen H, et al. Therapeutic effects and metabolic spectrum of traditional Chinese medicine hengqing II prescription on alzheimer's disease. *Evid Based Complement Alternat Med*. 2022;2022:5912396. doi:10.1155/2022/5912396
31. He Z, Li X, Han S, et al. Bis(ethylmaltolato)oxidovanadium (IV) attenuates amyloid-beta-mediated neuroinflammation by inhibiting NF- κ B signaling pathway via a PPAR γ -dependent mechanism. *Metallomics*. 2021;3:137. doi:10.1093/mtomcs/mfab036
32. Wang A, Wan X, Zhuang P, et al. High fried food consumption impacts anxiety and depression due to lipid metabolism disturbance and neuroinflammation. *Proc Natl Acad Sci U S A*. 2023;12018:e2221097120. doi:10.1073/pnas.2221097120
33. Li Y, Lei Z, Ritzel RM, et al. Impairment of autophagy after spinal cord injury potentiates neuroinflammation and motor function deficit in mice. *Theranostics*. 2022;12(12):5364–5388. doi:10.7150/thno.72713
34. Tao W, Hu Y, Chen Z, et al. Magnolol attenuates depressive-like behaviors by polarizing microglia towards the M2 phenotype through the regulation of Nrf2/HO-1/NLRP3 signaling pathway. *Phytomedicine*. 2021;91:153692. doi:10.1016/j.phymed.2021.153692
35. Cutolo M, Campitiello R, Gotelli E, et al. The role of M1/M2 macrophage polarization in rheumatoid arthritis synovitis. *Front Immunol*. 2022;13:867260. doi:10.3389/fimmu.2022.867260
36. Luo L, Liu M, Fan Y, et al. Intermittent theta-burst stimulation improves motor function by inhibiting neuronal pyroptosis and regulating microglial polarization via TLR4/NF κ B/NLRP3 signaling pathway in cerebral ischemic mice. *J Neuroinflammation*. 2022;19(1):141. doi:10.1186/s12974-022-02501-2
37. Prashantha Kumar BR, Kumar AP, Jose JA, et al. Minutes of PPAR- γ agonism and neuroprotection. *Neurochem Int*. 2020;140:104814. doi:10.1016/j.neuint.2020.104814
38. Tang J, Xu L, Zeng Y, et al. Effect of gut microbiota on LPS-induced acute lung injury by regulating the TLR4/NF- κ B signaling pathway. *Int Immunopharmacol*. 2021;91:107272. doi:10.1016/j.intimp.2020.107272
39. Lepetos P, Papavassiliou KA, Papavassiliou AG. Redox and NF- κ B signaling in osteoarthritis. *Free Radic Biol Med*. 2019;132:90–100. doi:10.1016/j.freeradbiomed.2018.09.025
40. Wei Z, Li D, Shi J. Alterations of spatial memory and gut microbiota composition in alzheimer's disease triple-transgenic mice at 3, 6, and 9 months of age. *Am J Alzheimers Dis Other Dement*. 2023;38:15333175231174193. doi:10.1177/15333175231174193
41. Aldana BI, Zhang Y, Jensen P, et al. Glutamate-glutamine homeostasis is perturbed in neurons and astrocytes derived from patient iPSC models of frontotemporal dementia. *Mol Brain*. 2020;13(1):125. doi:10.1186/s13041-020-00658-6
42. Andersen JV, Markussen KH, Jakobsen E, et al. Glutamate metabolism and recycling at the excitatory synapse in health and neurodegeneration. *Neuropharmacology*. 2021;196:108719. doi:10.1016/j.neuropharm.2021.108719
43. Adaikkan C, Middleton SJ, Marco A, et al. Gamma entrainment binds higher-order brain regions and offers neuroprotection. *Neuron*. 2019;1025:929–943.e8. doi:10.1016/j.neuron.2019.04.011
44. Bekdash RA, Bronsert P, Poc M. The cholinergic system, the adrenergic system and the neuropathology of alzheimer's disease. *Int J Mol Sci*. 2021;23(1):223. doi:10.3390/ijms23010223
45. Majidi A, Sadigh-Eteghad S, Rahigh Aghsan S, et al. Amyloid- β , tau, and the cholinergic system in Alzheimer's disease: seeking direction in a tangle of clues. *Rev Neurosci*. 2020;314(4):391–413. doi:10.1515/revneuro-2019-0089
46. Pinz MP, Vogt AG, da Costa Rodrigues K, et al. Effect of a purine derivative containing selenium to improve memory decline and anxiety through modulation of the cholinergic system and Na(+)/K(+)-ATPase in an Alzheimer's disease model. *Metab Brain Dis*. 2021;365(5):871–888. doi:10.1007/s11011-021-00703-w
47. Yan YP, Chen JY, Lu JH. Disease-modifying activity of huperzine a on alzheimer's disease: evidence from preclinical studies on rodent models. *Int J Mol Sci*. 2022;23(4):2323. doi:10.3390/ijms23042323
48. Scheltens P, De Strooper B, Kivipelto M, et al. Alzheimer's disease. *Lancet*. 2021;39710284(10284):1577–1590. doi:10.1016/S0140-6736(20)32205-4
49. Tiwari S, Atluri V, Kaushik A, et al. Alzheimer's disease: pathogenesis, diagnostics, and therapeutics. *Int J Nanomed*. 2019;14:5541–5554. doi:10.2147/IJN.S200490
50. Ashrafiyan H, Zadeh EH, Khan RH. Review on Alzheimer's disease: inhibition of amyloid beta and tau tangle formation. *Int J Biol Macromol*. 2021;167:382–394. doi:10.1016/j.ijbiomac.2020.11.192
51. Andrade S, Loureiro JA, Pereira MDC. Influence of in vitro neuronal membranes on the anti-amyloidogenic activity of gallic acid: implication for the therapy of Alzheimer's disease. *Arch Biochem Biophys*. 2021;711:109022. doi:10.1016/j.abb.2021.109022
52. Mori T, Koyama N, Yokoo T, et al. Gallic acid is a dual α/β -secretase modulator that reverses cognitive impairment and remediates pathology in Alzheimer mice. *J Biol Chem*. 2020;29548(48):16251–16266. doi:10.1074/jbc.RA119.012330
53. Yu M, Chen X, Liu J, et al. Gallic acid disruption of A β (1-42) aggregation rescues cognitive decline of APP/PS1 double transgenic mouse. *Neurobiol Dis*. 2019;124:67–80. doi:10.1016/j.nbd.2018.11.009
54. Thakur S, Dhapola R, Sarma P, et al. Neuroinflammation in alzheimer's disease: current progress in molecular signaling and therapeutics. *Inflammation*. 2023;46(1):1–17. doi:10.1007/s10753-022-01721-1
55. Zhou R, Ji B, Kong Y, et al. PET imaging of neuroinflammation in alzheimer's disease. *Front Immunol*. 2021;12:739130. doi:10.3389/fimmu.2021.739130
56. Law SH, Chan ML, Marathe GK, et al. An updated review of lysophosphatidylcholine metabolism in human diseases. *Int J Mol Sci*. 2019;3:205. doi:10.3390/ijms20051149
57. Freeman L, Guo H, David CN, et al. NLR members NLR4 and NLRP3 mediate sterile inflammasome activation in microglia and astrocytes. *J Exp Med*. 2017;2145(5):1351–1370. doi:10.1084/jem.20150237
58. Alam J, Sharma L. Potential enzymatic targets in alzheimer's: a comprehensive review. *Curr Drug Targets*. 2019;203:316–339. doi:10.2174/1389450119666180820104723

59. Sarkar C, Jones JW, Hegdekar N, et al. PLA2G4A/cPLA2-mediated lysosomal membrane damage leads to inhibition of autophagy and neurodegeneration after brain trauma. *Autophagy*. 2020;163(3):466–485. doi:10.1080/15548627.2019.1628538
60. Kurano M, Saito Y, Uranbileg B, et al. Modulations of bioactive lipids and their receptors in postmortem Alzheimer's disease brains. *Front Aging Neurosci*. 2022;14:1066578. doi:10.3389/fnagi.2022.1066578
61. Li N, Liu Y, Li W, et al. A UPLC/MS-based metabolomics investigation of the protective effect of ginsenosides Rg1 and Rg2 in mice with Alzheimer's disease. *J Ginseng Res*. 2016;401(1):9–17. doi:10.1016/j.jgr.2015.04.006
62. Sheikh AM, Michikawa M, Kim SU, et al. Lysophosphatidylcholine increases the neurotoxicity of Alzheimer's amyloid β 1-42 peptide: role of oligomer formation. *Neuroscience*. 2015;292:159–169. doi:10.1016/j.neuroscience.2015.02.034
63. Sheikh AM, Nagai A. Lysophosphatidylcholine modulates fibril formation of amyloid beta peptide. *Febs j*. 2011;2784(4):634–642. doi:10.1111/j.1742-4658.2010.07984.x
64. Liu T, Wang X, Guo F, et al. Lysophosphatidylcholine induces apoptosis and inflammatory damage in brain microvascular endothelial cells via GPR4-mediated NLRP3 inflammasome activation. *Toxicol In Vitro*. 2021;77:105227. doi:10.1016/j.tiv.2021.105227
65. Sun E, Motolani A, Campos L, et al. The pivotal role of NF- κ B in the pathogenesis and therapeutics of alzheimer's disease. *Int J Mol Sci*. 2022;23(4):2316. doi:10.3390/ijms23042316
66. Zusso M, Lunardi V, Franceschini D, et al. Ciprofloxacin and levofloxacin attenuate microglia inflammatory response via TLR4/NF- κ B pathway. *J Neuroinflammation*. 2019;161(1):148. doi:10.1186/s12974-019-1538-9
67. Nguyen PL, Bui BP, Lee H, et al. A Novel 1,8-Naphthyridine-2-Carboxamide Derivative Attenuates Inflammatory Responses and Cell Migration in LPS-Treated BV2 Cells via the Suppression of ROS Generation and TLR4/Myd88/NF- κ B Signaling Pathway. *Int J Mol Sci*. 2021;23(1):225. doi:10.3390/ijms23010225
68. Kumar AP, Kumar BRP, Kumar BRP, et al. Glitazones, PPAR- γ and Neuroprotection. *Mini Rev Med Chem*. 2021;2112(12):1457–1464. doi:10.2174/1389557521666210304112403
69. Dhapola R, Hota SS, Sarma P, et al. Recent advances in molecular pathways and therapeutic implications targeting neuroinflammation for Alzheimer's disease. *Inflammopharmacology*. 2021;296(6):1669–1681. doi:10.1007/s10787-021-00889-6
70. Li Q, Sun J, Mohammadtursun N, et al. Curcumin inhibits cigarette smoke-induced inflammation via modulating the PPAR γ -NF- κ B signaling pathway. *Food Funct*. 2019;1012(12):7983–7994. doi:10.1039/C9FO02159K
71. Wang J, Xu X, Li P, et al. HDAC3 protects against atherosclerosis through inhibition of inflammation via the microRNA-19b/PPAR γ /NF- κ B axis. *Atherosclerosis*. 2021;323:1–12. doi:10.1016/j.atherosclerosis.2021.02.013
72. Ju Z, Su M, Hong J, et al. Anti-inflammatory effects of an optimized PPAR- γ agonist via NF- κ B pathway inhibition. *Bioorg Chem*. 2020;96:103611. doi:10.1016/j.bioorg.2020.103611
73. Lei Y, Hou F, Wu X, et al. Brucine-induced neurotoxicity by targeting caspase 3: involvement of PPAR γ /NF- κ B/Apoptosis signaling pathway. *Neurotox Res*. 2022;406(6):2117–2131. doi:10.1007/s12640-022-00581-9

Drug Design, Development and Therapy

Dovepress

Publish your work in this journal

Drug Design, Development and Therapy is an international, peer-reviewed open-access journal that spans the spectrum of drug design and development through to clinical applications. Clinical outcomes, patient safety, and programs for the development and effective, safe, and sustained use of medicines are a feature of the journal, which has also been accepted for indexing on PubMed Central. The manuscript management system is completely online and includes a very quick and fair peer-review system, which is all easy to use. Visit <http://www.dovepress.com/testimonials.php> to read real quotes from published authors.

Submit your manuscript here: <https://www.dovepress.com/drug-design-development-and-therapy-journal>